HEALTH AND MEDICINE

Nanoparticle-based inhibition of vascular endothelial growth factor receptors alleviates osteoarthritis pain and cartilage damage

Kaige Ma[1]†, Tiep Pham[1,2]†, Jun Wang[1]†, InSug O-Sullivan[1], Amy DiCamillo[3], Shiyu Du[1,2], Fackson Mwale[4], Zeba Farooqui[1], Gina Votta-Velis[5], Benjamin Bruce[6], Andre J. van Wijnen[1,7], Ying Liu[1,2,8]*, Hee-Jeong Im[1,6]*

Osteoarthritis (OA) is characterized by cartilage damage, inflammation, and pain. Vascular endothelial growth factor receptors (VEGFRs) have been associated with OA severity, suggesting that inhibitors targeting these receptors alleviate pain (via VEGFR1) or cartilage degeneration (via VEGFR2). We have developed a nanoparticle-based formulation of pazopanib (Votrient), an FDA-approved anticancer drug that targets both VEGFR1 and VEGFR2 (Nano-PAZII). We demonstrate that a single intraarticular injection of Nano-PAZII can effectively reduce joint pain for a prolonged time without substantial side effects in two different preclinical OA rodent models involving either surgical (upon partial medial meniscectomy) or nonsurgical induction (with monoiodoacetate). The injection of Nano-PAZII blocks VEGFR1 and relieves OA pain by suppressing sensory neuronal ingrowth into the knee synovium and neuronal plasticity in the dorsal root ganglia and spinal cord. Simultaneously, the inhibition of VEGFR2 reduces cartilage degeneration. These findings provide a mechanism-based disease-modifying drug strategy that addresses both pain symptoms and cartilage loss in OA.

INTRODUCTION

Osteoarthritis (OA) and other degenerative cartilage disorders are leading causes of chronic pain, resulting from cartilage damage and inflammation (*1*–*6*). The prevalence of knee OA, which affects millions of people globally, has steeply increased due to increased life expectancy and the rise of metabolic disorders (e.g., obesity) that exacerbate OA risk. OA pain symptoms heavily affect the quality of life and health care, yet there are no effective or clinically approved treatment strategies that can mitigate or prevent disease progression or manage OA-specific pain (*2*, *3*). Therefore, there is an urgent need to identify previously unknown therapeutic targets and validate unique disease-modifying osteoarthritis drugs (DMOADs) to inhibit both chronic joint pain and pathologic progression of cartilage degeneration and nerve modifications.

Elevated vascular endothelial growth factor (VEGF) levels and the formation of new blood vessels in joints are pathologically associated with OA joint pain (*7*–*9*). Several VEGF ligands (e.g., VEGFA, VEGFB, and VEGFC) might play a part during OA progression and pain (*10*, *11*). Direct evidence for the role of VEGFs suggests that intraarticular (IA) injection of VEGFs into the knee joint mimics OA-like joint pathology and inhibition of VEGF signaling retards OA progression (*12*–*16*). These ligands converge on two cognate cell surface receptors (e.g., VEGFR1/FLT1 and VEGFR2/FLK1) that have mechanistically distinct pathological roles: VEGFR1 is primarily responsible for joint pain transmission, while VEGFR2 is linked to cartilage degeneration (*15*). Therefore, the simultaneous inhibition of both receptors represents a very attractive two-pronged strategy for OA treatment.

Pazopanib targets both VEGFR1 and VEGFR2 and belongs to a wider class of US Food and Drug Administration (FDA)–approved small molecules that act as tyrosine kinase inhibitors of VEGFR1/2 receptors (e.g., axitinib, cabozantinib, lenvatinib, sorafenib, sunitinib, and pazopanib). These agents represent adenosine triphosphate analogs that are steady-state competitive inhibitors of the active site of the tyrosine kinase domain (*17*). However, several notable challenges hinder the clinical translation of the concept that pazopanib targets both VEGFR1-mediated pain and VEGFR2-mediated cartilage degeneration. First, pinpointing the optimal OA stage for VEGFR1 and VEGFR2 (e.g., post-injury, early OA, and advanced stages) dual inhibition is vital. Second, our prior research indicated that VEGFR inhibitors (e.g., pazopanib) require consistent drug injections (twice per week) for knee OA therapy (*15*). The frequency is clinically undesirable due to increased infection risk and other adverse effects (e.g., soft tissue damage), as well as the requirement for repetitive hospital visits and patient compliance (*18*, *19*). The biological half-life of pazopanib is 31.9 hours, and daily dosing has been recommended clinically (*20*, *21*). Reduction of OA pain by IA injection of pazopanib lasts only for 1 to 2 days in our preclinical animal model (*15*). Hence, reduction in the dosing frequency of pazopanib requires consideration of delivery methods that prolong the bioavailability of pazopanib.

The development of a controlled, slow-release system for active pharmaceutical ingredients (API) compliant with FAD standards is critical for the successful local (IA) delivery of drugs, especially for APIs with short half-lives. Benefits include (i) less frequent drug injections; (ii) reduced fluctuations in steady-state drug levels; (iii) improved management of disease conditions through controlled release; and (iv) increased safety margins for high-potency drugs due

[1]Department of Biomedical Engineering, University of Illinois at Chicago, Chicago, IL 60607, USA. [2]Department of Chemical Engineering, University of Illinois at Chicago, Chicago, IL 60608, USA. [3]Melior Discovery Inc., 869 Springdale Drive 500, Exton, PA 19341, USA. [4]Orthopaedic Research Laboratory, Lady Davis Institute for Medical Research, SMBD-Jewish General Hospital, McGill University, Montreal, Canada. [5]Department of Anesthesiology, University of Illinois at Chicago, Chicago, IL 60612, USA. [6]Jesse Brown Veterans Affairs Medical Center (JBVAMC) at Chicago, IL 60612, USA. [7]Department of Biochemistry, University of Vermont, Burlington, VT 05405, USA. [8]Department of Pharmaceutical Sciences, University of Illinois at Chicago, Chicago, IL 60612, USA.
*Corresponding author. Email: hsampe2@uic.edu (H.-J.I.); liuying@uic.edu (Y.L.)
†These authors contributed equally to this work.

to both local delivery and slow release of the drug. Here, we demonstrate that nanoparticle-based sustained delivery of the VEGFR inhibitor pazopanib (Nano-PAZII) via a single IA injection permits the reversal of OA symptoms in different stages of experimental OA. These findings position Nano-PAZII as a viable and innovative disease-modifying drug strategy for OA.

RESULTS

Encapsulation of pazopanib into nanoparticles supports drug retention and release

IA injection of pazopanib rapidly alleviates OA pain for more than 2 days in preclinical murine OA models (*15*). However, sustained inhibition beyond this period requires a bi-weekly IA injection, a frequency deemed undesirable in clinical settings. To improve upon this, we developed a nanotechnology-based formulation of pazopanib (Nano-PAZII) designed to extend joint pain relief for several months after just a single IA injection (Fig. 1). Using a biomaterial-based strategy for sustained drug release and prolonged drug retention (Figs. 2 and 3), we aimed to maintain VEGFR1/VEGFR2 inhibition via pazopanib in the synovial space of the joint (Fig. 4) and reverse OA symptoms. Doses up to 2.25 μg/ml (5.1 μM) of pazopanib are safely tolerated in vitro and show potential to mitigate interleukin-1β (IL-1β/IL1B)-mediated lactate dehydrogenase (LDH) release in primary human chondrocyte and fibroblast-like synoviocyte (FLS) culture models (fig. S1). Pazopanib promotes chondrocyte extracellular matrix integrity by suppressing expression of catabolic genes (*MMP13* and *RUNX2*) and increasing expression of anabolic genes (*COL2A1* and *ACAN*) in primary human chondrocyte cultures under inflammatory conditions (e.g., VEGFA or IL-1β/IL1B stimulation) and may also help in reducing pain and inflammatory markers (*NGF* and *VEGFR1*) in primary human FLSs (fig. S2). Thus, pazopanib represents a potential OA disease–modifying drug that may protect knee joints from cartilage degeneration while potentially immediately relieving OA pain.

In our study, we created a slow-release formulation of pazopanib (Nano-PAZII) by encapsulating the drug in polymeric nanoparticles of a diblock copolymer [polyethylene glycol-*b*-polycaprolactone amphiphilic diblock copolymer (PEG-*b*-PCL)] using flash nanoprecipitation (FNP) (*22*). The precipitation kinetics of FNP were initially optimized by adjusting the concentrations of the drug and polymer, as well as by selecting distinct polymer blocks with different molecular weights. During FNP, drug and particles were rapidly mixed at a 1:1 mass ratio in the organic phase [dimethyl sulfoxide (DMSO)] using a custom-made multi-inlet vortex mixer. Nanoparticles were then generated by combining this mixture with an aqueous phase (i.e., deionized water as antisolvent) to drive encapsulation via hydrophobic interactions between pazopanib and hydrophobic segments in the polymer, as well as the concomitant self-assembly of PEG-*b*-PCL micelles. Optimization of Nano-PAZII formulations (Fig. 2A) permits initial drug loading of up to half-maximal efficiency (~50%) with near-maximal drug encapsulation efficiency

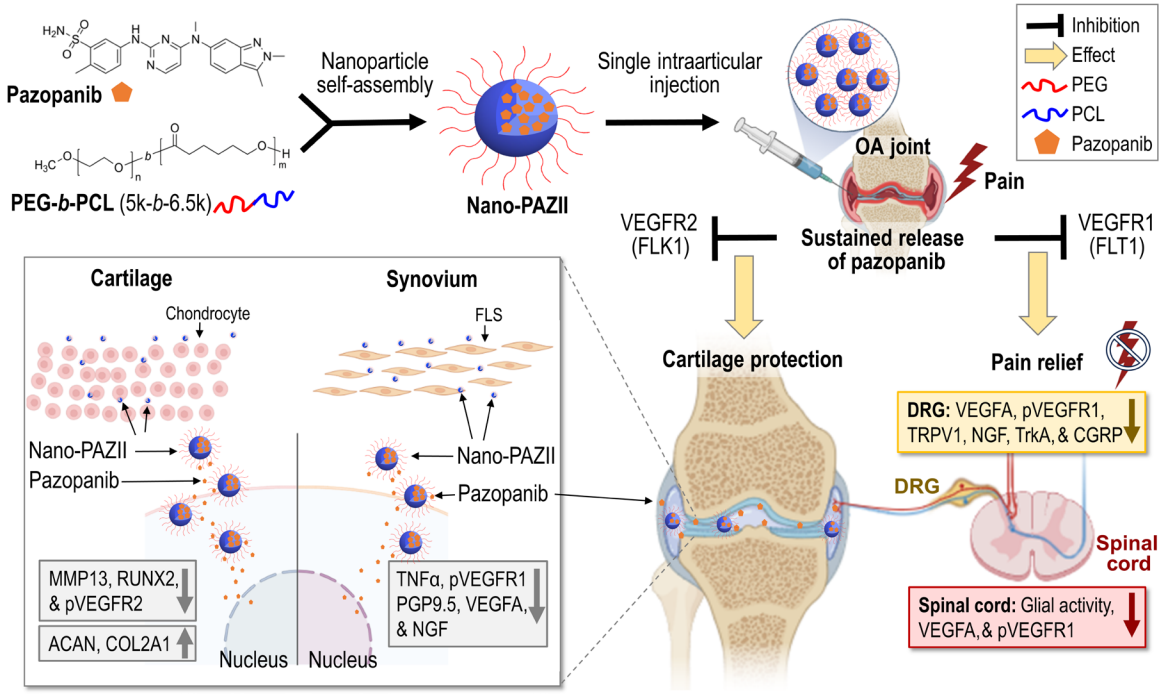

Fig. 1. Schematic illustration of a single IA injection of pazopanib nano-formulation (Nano-PAZII) for long-term OA treatment. The diagram shows the encapsulation of pazopanib (top left) into polymeric nanoparticles (PEG-*b*-PCL) by flash nanoprecipitation (FNP) to generate Nano-PAZII (top middle). A single IA injection of Nano-PAZII (top right) suffices for the rapid and sustained reduction of knee joint pain. The therapeutic effects of Nano-PAZII are attributable to inhibition of VEGFR1/FLT1, which relieves chronic OA pain, and inhibition of VEGFR2/FLK1, which protects cartilage from OA-related degradation (bottom right), consistent with our previous studies (*15*). At the cellular level, pazopanib released by Nano-PAZII in cartilage and synovium (bottom left) reduces negative biomarkers (e.g., inflammatory, neural, and cartilage catabolic factors) and increases positive biomarkers (e.g., cartilage extracellular matrix proteins). PCL, poly caprolactone-hydrophobic segment; PEG, polyethylene glycol-hydrophilic segment; FLSs, fibroblast-like synoviocytes; DRG, dorsal root ganglia.

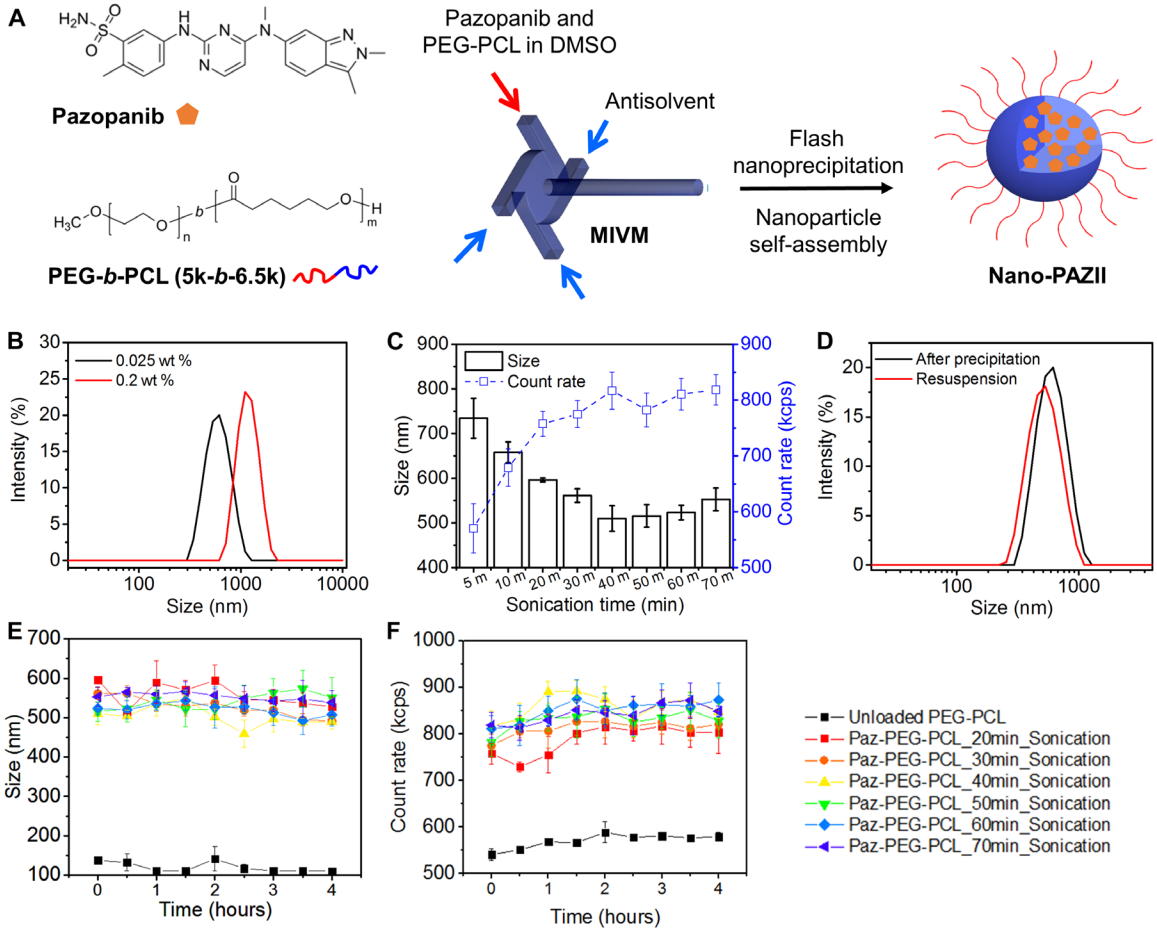

Fig. 2. Formation and characterization of the PEG-*b*-PCL nanoparticles with and without encapsulation of pazopanib. (**A**) Diagram showing encapsulation of pazopanib in PEG-*b*-PCL nanoparticles (Nano-PAZII), PCL (blue line), and PEG (red line). The hydrophobic drug pazopanib and the amphiphilic diblock copolymer PEG-*b*-PCL were molecularly dissolved in DMSO. Upon flash mixing with an antisolvent (marked by blue arrows) in the multi-inlet vortex mixer (the inlet stream of pazopanib and PEG-*b*-PCL in DMSO marked by the red arrow), the drug compound and the polymer self-assembled into the nanoparticles. (**B**) Size distribution of the nanoparticles after precipitation at initial concentrations (0.2 or 0.025 wt %) for both pazopanib and the polymer. (**C**) Size measurements of the resuspended nanoparticles as a function of sonication time. (**D**) Size distribution of the nanoparticles generated immediately after FNP and after resuspension after 40-min sonication. Nanoparticles were resuspended in PBS buffer after various sonication times as indicated (20, 30, 40, 50, 60, and 70 min, respectively). The average sizes of nanoparticles (**E**) and light-scattering photon count rate (**F**) were used to characterize the 4-hour stability of the nanoparticles in PBS buffer.

(~100%). Preparations with large particles (>1000 nm) produced at 0.2 wt % initial drug concentration exhibit visible aggregations within the first few hours of dialysis. However, smaller particle sizes (~600 nm) that form at an eightfold lower initial drug concentration of 0.025 wt % do not have this limitation (Fig. 2B). Therefore, the 0.025% formulation was selected for further studies. After dialysis and lyophilization, the dried nanoparticle formulation was collected as a powder and stored at −20°C for long-term storage. Before dosing in animals, nanoparticles were resuspended in phosphate-buffered saline (PBS) buffer at a drug concentration of 6.5 mg/ml (14.9 mM). The size of the resuspended nanoparticles appears to depend on the sonication time (Fig. 2C), and the nanoparticles have a similar size distribution as particles generated immediately after FNP (Fig. 2D). The final drug loading and encapsulation efficiencies of the resuspended particles are 20 and 70%, respectively. The empty PEG-*b*-PCL nanoparticles without drug encapsulation exhibit a size of around 100 nm (Fig. 2E). Four-hour stability after resuspension was monitored to ensure that there would be sufficient time between preparation of the suspension and injection. All samples remain stable for 4 hours with size fluctuations of less than 10% (Fig. 2, E and F). Collectively, these procedures yielded pazopanib nanoparticles of about 200 to 1000 nm, designed for local drug release and limited systemic circulation.

Nanoparticles release pazopanib with pH-dependent zero-order kinetics in vitro

The bioavailability of pazopanib is influenced by the pH-dependent release from PEG-based nanoparticles (see Materials and Methods). Therefore, the in vitro drug release was measured in buffer solutions with different degrees of acidity (pH = 3 and pH = 5) at 37°C. The cumulative release of pazopanib steadily increases over 17 weeks, and most of pazopanib (>70%) is released from the nanoparticles at pH = 3, but pazopanib release is limited at pH = 5 (<3%) (Fig. 3A). The relative release rate of pazopanib decreased over time, but the

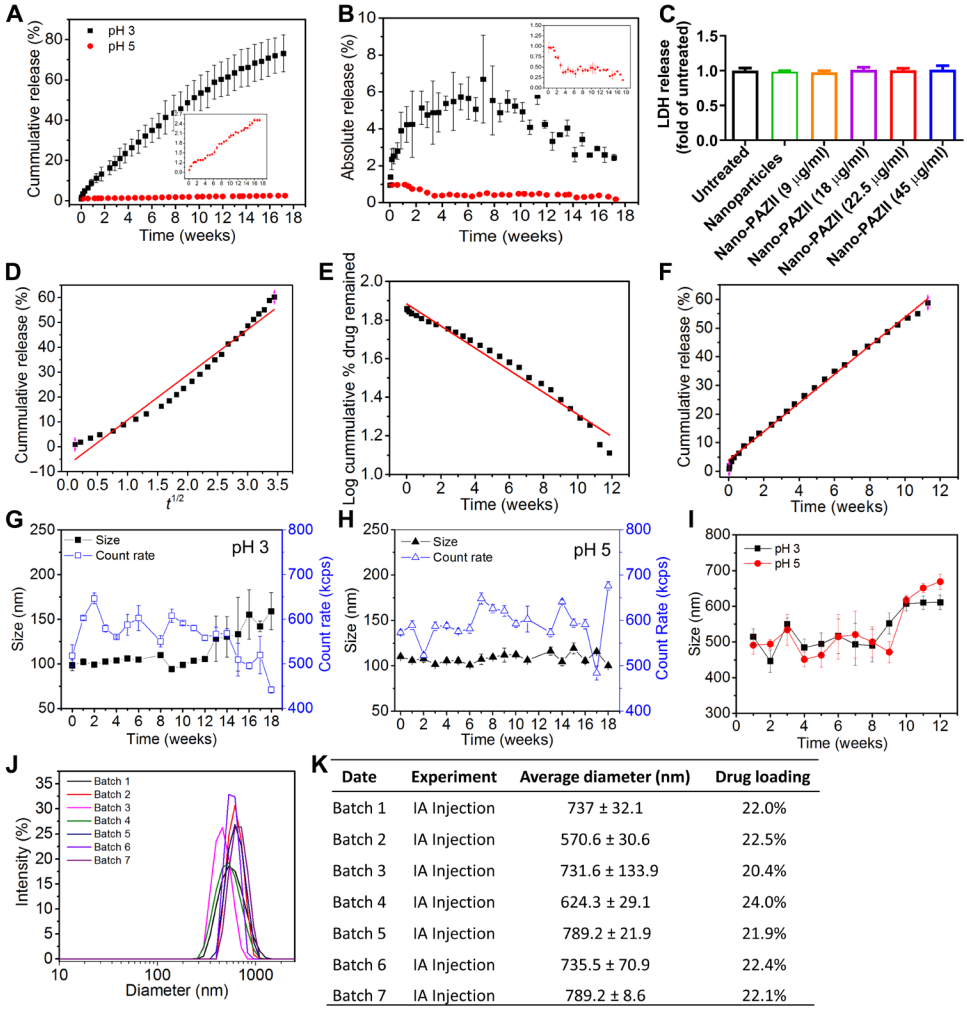

K

Date	Experiment	Average diameter (nm)	Drug loading
Batch 1	IA Injection	737 ± 32.1	22.0%
Batch 2	IA Injection	570.6 ± 30.6	22.5%
Batch 3	IA Injection	731.6 ± 133.9	20.4%
Batch 4	IA Injection	624.3 ± 29.1	24.0%
Batch 5	IA Injection	789.2 ± 21.9	21.9%
Batch 6	IA Injection	735.5 ± 70.9	22.4%
Batch 7	IA Injection	789.2 ± 8.6	22.1%

Fig. 3. In vitro release, degradation, and reproducibility of pazopanib-loaded PEG-*b*-PCL nanoparticles (Nano-PAZII). The amount of pazopanib was quantified using high-performance liquid chromatography (HPLC) and plotted as cumulative percent release (**A**) or absolute percent release (**B**) at pH = 3 or pH = 5 at 37°C; the inset in (A) shows results at pH = 5 on a different scale. In vitro cytotoxicity of Nano-PAZII was determined by measuring the cell viability of primary human chondrocytes after coincubation with Nano-PAZII at various concentrations. Statistical analyses were performed using unpaired *t* tests. Data are presented as means ± SEM (**C**). Model fitting of the release kinetics of Nano-PAZII in pH = 3 buffer. In vitro release of pazopanib from the PEG-*b*-PCL nanoparticles was fitted with Higuchi model with $R^2 = 0.9672$ (**D**), first-order model with $R^2 = 0.9731$ (**E**), and zero-order kinetics model with $R^2 = 0.9956$ (**F**). The sizes and photon count rates were determined by DLS over time for unloaded PEG-*b*-PCL nanoparticles suspended in buffers with pH = 3 (**G**) or pH = 5 (**H**); nanoparticle size and scattered photon count remain comparable for the first 13 weeks, indicating slow in vitro degradation of the polymeric nanoparticles. Sizes of pazopanib-loaded PEG-*b*-PCL nanoparticles were determined at pH = 3 and pH = 5 (**I**). Reproducibility analyses of Nano-PAZII of multiple batches for mouse articular (IA) injection with particle size distributions measured by DLS (**J**) and drug loading quantified by HPLC is shown in table (**K**).

most significant amount of released pazopanib occurred around week 8 (Fig. 3B). Furthermore, chondrocytes treated with Nano-PAZII for 16 hours retained their viability and did not release excessive LDH with nanoparticles containing pazopanib concentrations up to 45 μg/ml (Fig. 3C). Nano-PAZII demonstrated a favorable zero-order kinetic release profile that is independent of initial compound concentrations and exhibits minimum burst release depending on the pH (Fig. 3, D to F), consistent with previous studies on insulin and curcumin release from PEG-*b*-PCL (*23*, *24*). This suggests that Nano-PAZII is well tolerated by chondrocytes and is physiologically biocompatible.

During our study, we observed that both loaded and unloaded PEG-*b*-PCL nanoparticles remained stable across different pH levels (pH = 3 or pH = 5) for approximately 11 weeks, as reflected in the size distributions and photon count rate of the dynamic light scattering (DLS) (Fig. 3, G to I). The pazopanib-loaded particles are typically larger than unloaded particles; however, significant aggregation was only observed for unloaded particles after 14 weeks at pH = 3 (Fig. 3G). The Nano-PAZII particles only displayed a modest increase in size (~25%) after 11 weeks (Fig. 3I). The increase in size is usually resulted from the nonlinear coupling effects of molecule transport and particle collision. In this case, the modest growth in particle size after 11 weeks may be attributed to particle degradation and Ostwald ripening (i.e., partially degraded nanoparticles are re-adsorbed by adjacent particles at a timescale that is notably slower than random particle aggregation)

(*25*). Multiple batches of Nano-PAZII exhibited consistent size distributions (Fig. 3, J and K), indicating acceptable reproducibility for soft-matter polymeric nanoparticles. Collectively, the slow drug release kinetics, stable particle size distribution, and reproducible manufacturing of Nano-PAZII permit reliable predictions of drug compound pharmacokinetics and efficacy. These essential features render Nano-PAZII ideal for treating OA as a chronic disease by minimizing the number of required injections to obtain sustained inhibition of VEFGR1 and VEGFR2 in the synovial space.

Nano-PAZII offers extended pain relief during various OA stages

Because pazopanib targets VEGFR1, a known contributor to OA pain (*15*), we evaluated the pain relief potential of Nano-PAZII. Pain-related behavioral effects were assessed over 16 weeks postdrug administration at three OA stages: at 1 week (post-injury stage), 4 weeks (early OA stage), or 8 weeks (advanced OA stage) (Fig. 4, A and B, and fig. S3). The analgesic effects of a single IA injection of Nano-PAZII are also observed in a nonsurgical murine model in which OA is induced by the IA injection of the corrosive irritant monoiodoacetate (MIA) (fig. S4A). Tactile allodynia was used as a measure of pain sensitization and monitored by examining the withdrawal reflex of the mouse hindpaw upon application of gentle pressure (mechanical allodynia by von Frey filament testing) or the thermal reflex response of mice upon application of modest heat (thermal sensitivity by hot plate testing). Pain was quantitatively measured by assessing behavioral responses after applying gentle pressure (mechanical allodynia by von Frey filament testing) or modest heat (thermal sensitivity by hot plate testing) to the hindpaws. Both behavioral pain tests notably indicate that Nano-PAZII provides sustained relief of injury-induced OA pain upon injection at each of the three different OA stages upon injection of either a maximal volume (10 μl; 65 μg per knee) or half-maximal volume (5 μl) of Nano-PAZII (Fig. 4, C to H). Notably, Nano-PAZII injected within 1 week after surgery immediately ameliorates post-injury, and this analgesic effect is sustained for more than 16 weeks following a single IA injection (Fig. 4, C and D), while injection after 4 weeks provides rapid relief of pain due to traumatic injury-induced OA pain (Fig. 4, E and F). A single IA injection of pazopanib (7.5 μg per knee, 5 μl) could only alleviate pain for less than 3 days when it was administered at the post-injury stage (fig. S3). Furthermore, we found consistent antihyperalgesic effects of Nano-PAZII treatment at different stages of MIA-induced OA, with generally more pronounced antinociceptive effects when Nano-PAZII is administered earlier (fig. S4, B and C). While early intervention with Nano-PAZII yields more optimal results, the sustained effects on pain relief at any stage of OA progression are consistent with the rational design, particle stability, and drug release kinetics of Nano-PAZII (see Fig. 3). The results indicate that Nano-PAZII is a potent OA disease–modifying drug candidate that could be considered for preventive and/or early OA treatment strategies.

Nano-PAZII mitigates cartilage degeneration in OA murine models

Given its targeting of VEGFR2, which is associated with cartilage degeneration (*15*), we examined the therapeutic efficacy of a single IA injection of Nano-PAZII on cartilage integrity by histopathological analyses of mouse knee joint samples at 16 weeks post–partial medial meniscectomy (PMM). Pathological grading was quantified by several methods, including Osteoarthritis Research Society International (OARSI) scoring, measurement of cartilage thickness, and synovitis scoring. At 16 weeks post-PMM, cartilage degeneration was evident (Fig. 5A). The administration of Nano-PAZII, commencing 1 week after PMM, significantly reduces the OARSI, synovitis scores, and osteophyte formation (reflected by the osteophyte size and maturity), as well as prevents the decrease of cartilage thickness and reduces the $CD31^+$ vessels in synovium at different stages of OA (Fig. 5). We observed that a higher dose of a volume of 10 μl yields better OARSI scores and cartilage thickness than a volume of 5 μl (fig. S5). The latter finding implies that the pazopanib concentration released upon IA injection of 10 μl of Nano-PAZII (i.e., 65 μg per knee, 3.25 mg/kg for a 20-g mouse) is near a threshold concentration for efficacy and was selected for subsequent studies. Nano-PAZII also protects joints from cartilage degeneration when injected during early or advanced OA stages (Fig. 5, A and D). Notably, the protective effect is more pronounced during the post-injury stage, consistent with the pain results (see Fig. 4).

In addition, histological evaluations show that Nano-PAZII significantly diminishes OARSI values (fig. S4, D and F) and favorably modulates OA-related reductions in cartilage thickness (fig. S4, D and G) synovitis scores (fig. S4, E and H) and the presence of $CD31^+$ synovial vessels in MIA-induced OA (fig. S4, I and J). Hence, the results for nonsurgical MIA-induced OA (fig. S4) generally corroborate results obtained for PMM-induced surgical OA (see Fig. 5). In summary, results from both preclinical OA animal models (PMM and MIA) together demonstrate that Nano-PAZII has long-term analgesic effects, protects cartilage from trauma-induced degeneration, and suppresses neovascularization when administered at post-injury, early, or advanced OA stages.

Nano-PAZII mechanistically alters knee OA progression through molecular effects in both cartilage and synovium

Because the levels of VEGFR1 and VEGFR2 are increased in chondrocytes from patients with OA (*15*), we examined whether Nano-PAZII affects molecular signaling events downstream from VEGFR1 and VEGFR2 in the PMM-induced OA model (Fig. 6). Consistent with expectations, there is significant activation of VEGFR2 in the knee joint cartilage of OA mice as reflected by the detection of phosphorylated epitopes in its receptor (pVEGFR2) at 16 weeks post-PMM (Fig. 6A). Immunofluorescence microscopy analysis indicates that phosphorylation-mediated activation of both VEGFR2 in cartilage and VEGFR1 in knee synovium is suppressed by a single IA injection of Nano-PAZII at different stages of OA progression (Fig. 6, A and B). Matrix metalloproteinase-13 (*MMP13*) encodes the primary matrix metalloproteinase that mediates cartilage degradation, and *RUNX2* is an essential transcription factor that supports osteogenesis and chondrocyte hypertrophy. The data from IF staining indicate that Nano-PAZII significantly decreases MMP13, RUNX2, and tumor necrosis factor α (TNFα/TNF) protein levels in cartilage tissues (Fig. 6A) and TNFα/TNF protein levels in synovial tissues at different OA stages (Fig. 6B). This finding aligns with the concept that VEGFR2 activation in the OA knee joint is biologically linked to increased expression of cartilage catabolic and inflammatory factors, including MMP13, RUNX2, and TNFα/TNF, that play key roles in injury-induced cartilage degeneration. Our findings show that Nano-PAZII inhibits the OA-related activation of VEGFR2 and consequently reduces the expression of catabolic enzymes and inflammatory proteins in cartilage.

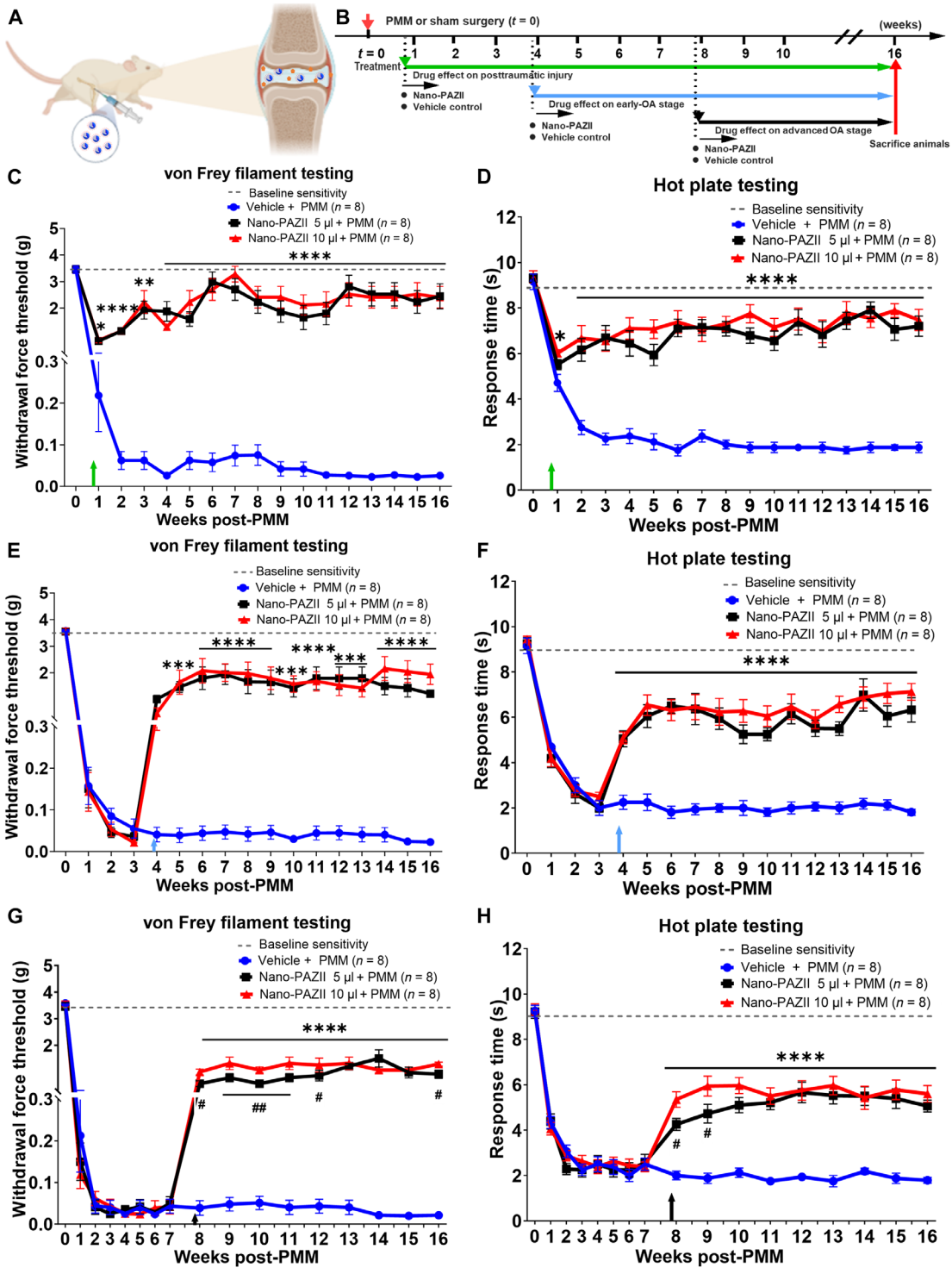

Fig. 4. Pain-related behavioral effects of a single IA injection of Nano-PAZII in murine PMM-induced OA model at different stages of OA disease progression. (**A**) Illustration of OA treatment by IA injection of Nano-PAZII in OA mice. Schematic diagram of the research plan for Nano-PAZII treatment in the partial medial meniscectomy (PMM) induced OA model. Single doses of either Nano-PAZII ($n = 8$) or nanoparticles without pazopanib ($n = 8$) were injected intraarticularly (low, 32.5 µg per knee in 5 µl or high, 65 µg per knee in 10 µl). (**B**) Drug treatments began at week 1 (post-injury stage), week 4 (early OA stage), or week 8 (advanced OA stage) after PMM. Development of mechanical allodynia (von Frey filament testing) and thermal pain (hot plate testing) in the ipsilateral hind paw was monitored in mice receiving Nano-PAZII in the post-injury stage (**C** and **D**), early OA stage (**E** and **F**), and advanced OA stage (**G** and **H**). The up arrow indicates the time of Nano-PAZII administration (C-H). Statistical analyses were performed using two-way ANOVA followed by the Tukey-Kramer test. Data are presented as means ± SEM (comparisons between groups with or without 65 µg per knee Nano-PAZII injection in mice that underwent PMM, degrees of statistical significance are indicated by asterisks, *$P < 0.05$, **$P < 0.01$, ***$P < 0.001$, ****$P < 0.0001$, between 32.5 and 65 µg per knee Nano-PAZII treatment in mice that underwent PMM, #$P < 0.05$, ##$P < 0.01$.

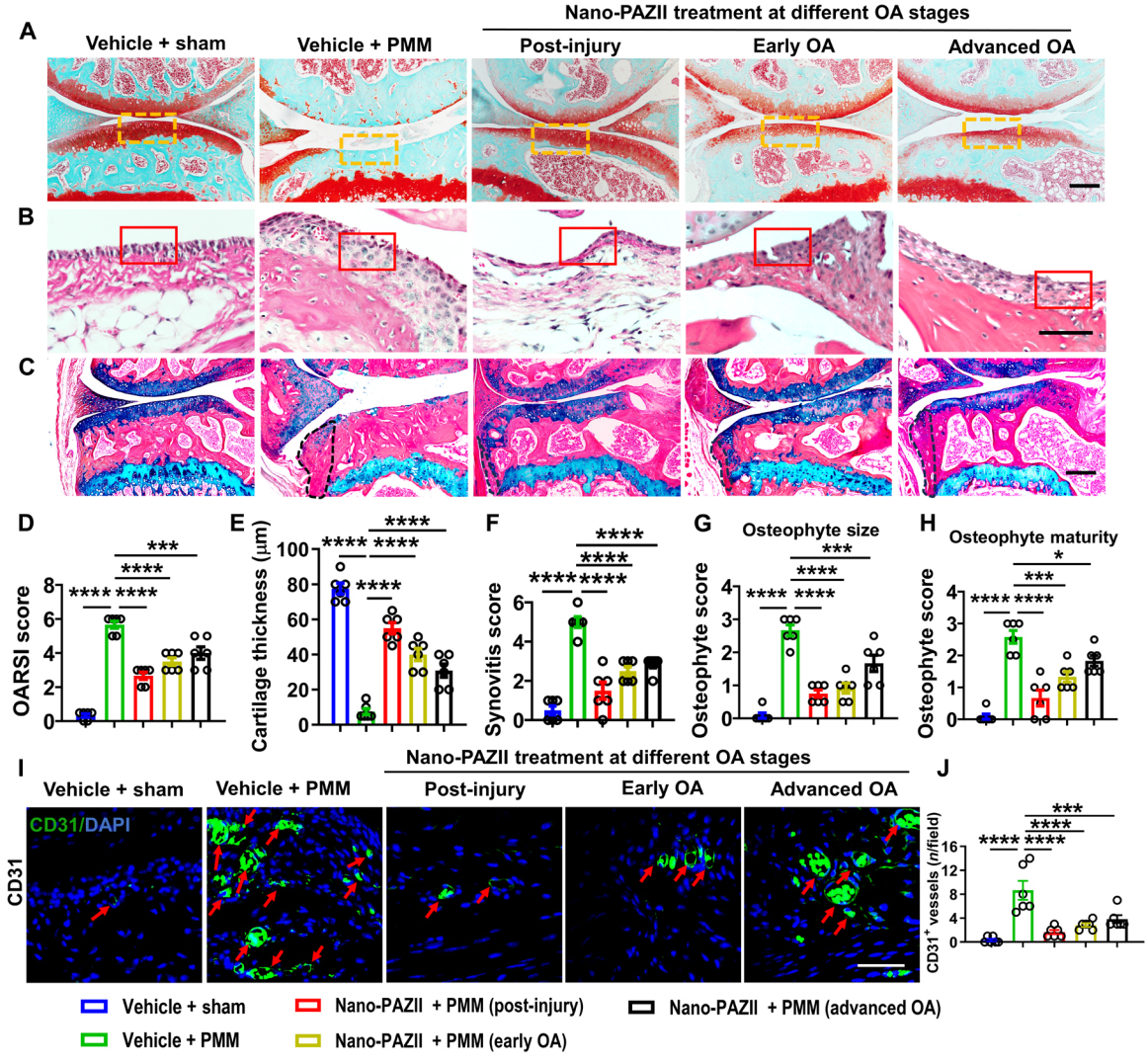

Fig. 5. Histopathological effects of a single IA injection of Nano-PAZII on joint tissue architecture. Mice with PMM received single IA injections of Nano-PAZII or vehicle as described above (see Fig. 4B). Representative images are presented for histological (**A** to **H**) and immunofluorescence analyses (**I** and **J**) at the three stages of OA progression after PMM (week 1: post-injury stage; week 4: early OA stage; week 8: advanced OA stage). Safranin O fast green staining of the knee joints reveals cartilage thickness (yellow boxed areas). Scale bar, 200 μm (A). Hematoxylin and eosin (H&E) staining of synovium tissue shows the synovial lining layer (red boxed areas). Scale bar, 100 μm (B). Alcian blue/hematoxylin and orange G (AB/H&OG) staining shows the osteophyte formation (black dashed line borders). Scale bar, 200 μm (C). Graphs of average OARSI scores, cartilage thickness, synovitis scores, and osteophyte formation including both size and maturity at the different stages of OA ($n = 6$) (D to H). Levels of CD31 in synovium were examined by immunofluorescence microscopy to detect $CD31^+$ blood vessels (red arrows). Scale bar, 100 μm (I). Quantitative results for the presence of $CD31^+$ vessels in the synovium ($n = 6$) (J). Data are presented as means ± SEM. Statistical analyses were performed using one-way analysis of variance (ANOVA) followed by the Dunnett multiple comparisons test. Comparisons were made between groups with or without Nano-PAZII treatment in mice that underwent PMM (*$P <$ 0.05, ***$P < 0.001$, and ****$P < 0.0001$).

One key pathological event during OA progression is the transition from asymptomatic to painful OA. This switch is linked to a VEGFA-related increase in the levels of nerve growth factor/tyrosine kinase receptor type A (NGF/TrkA) (*14*) that stimulate sensory neurite expansion (axonal outgrowth) in synovial knee joint tissues and dorsal root ganglia (DRG) sensory neurons (*14*). Notably, administering a single IA injection of Nano-PAZII at different OA stages prevents this VEGFA-dependent expansion of sensory neurites in knee joint tissues as determined by immunofluorescence microscopy (Fig. 6). Injection of Nano-PAZII, which blocks activation of VEGFR1 and VEGFR2 by VEGFA, significantly reduces protein signals for VEGFA, NGF, and VEGFR1 and the density of sensory nerve fibers (detected by PGP9.5, a neuronal marker that reflects sensory neurite distribution) in synovial tissues (Fig. 6). Considering the pain-related behaviors (Fig. 4) and histological findings (Fig. 5), it is evident that maximal efficacy of Nano-PAZII operates most effectively when the nanoparticles are administered during the early phases of OA (Fig. 6). Taken together, our results show that Nano-PAZII mediates both VEGFR1- and VEGFR2-related effects by reducing the expression of catabolic enzymes in cartilage while reducing the levels of inflammatory factors and distribution of sensory nerve fibers in knee synovium.

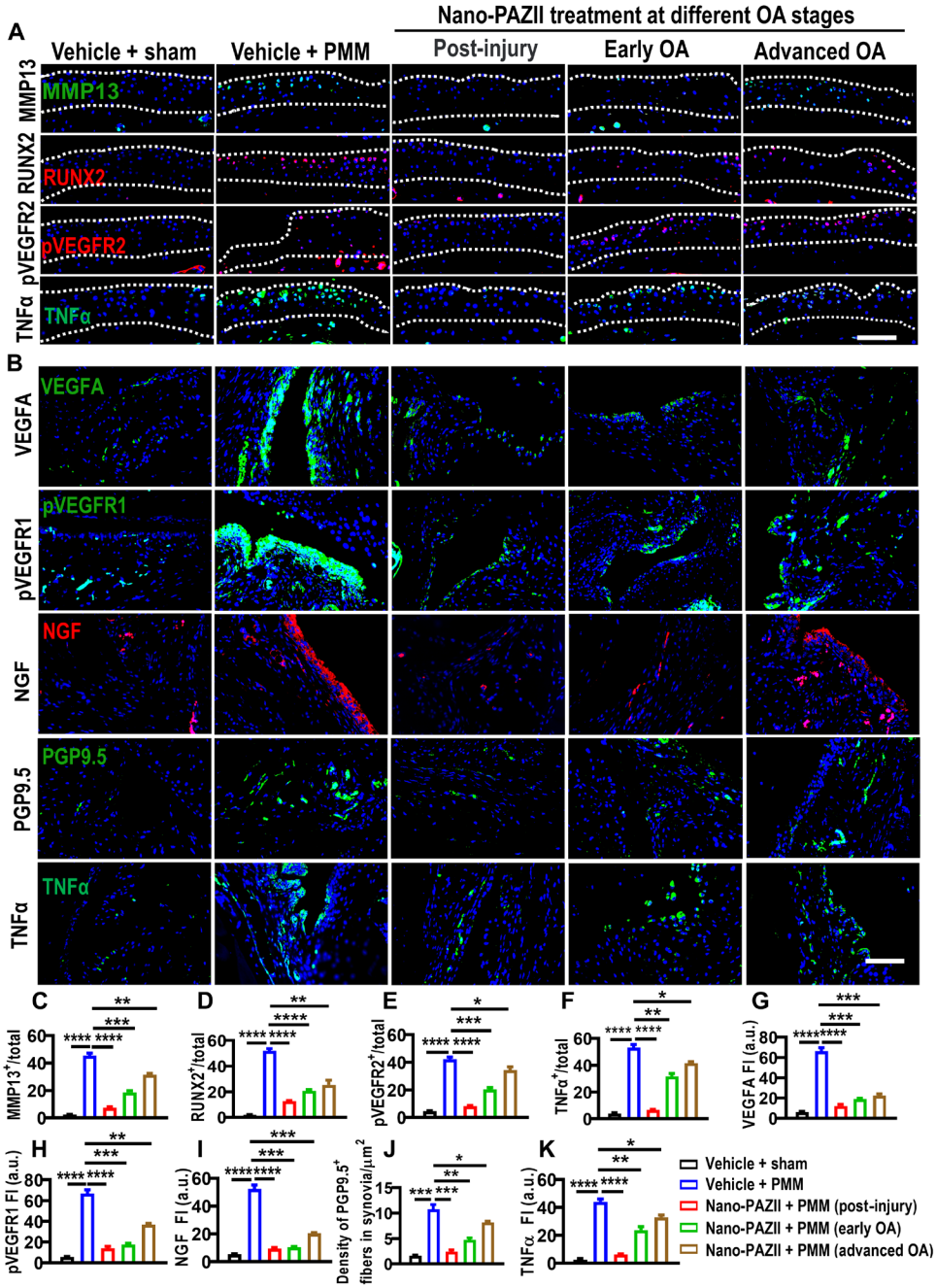

Fig. 6. Molecular and neurological effects of a single IA injection of Nano-PAZII. Immunofluorescence (IF) microscopy analyses were performed using histological sections of cartilage and synovial tissues in mice at 16 weeks after PMM. Nano-PAZII decreases levels of MMP13, RUNX2, phospho-VEGFR2 (pVEGFR2), and TNFα/TNF in cartilage (**A**) and peripheral nerve fiber sprouting in the synovium (**B**) during OA progression. The experimentation was carried out as described (see Fig. 4B) with a single IA injection of Nano-PAZII or vehicle at weeks 1, 4, and 8 after PMM. Levels of MMP13, TNFα/TNF (green), RUNX2, and pVEGFR2 (red) were examined in knee cartilage by IF microscopy (A). Levels of VEGFA, pVEGFR1, PGP9.5, TNFα/TNF (green), and NGF (red) in knee synovium were examined by IF microscopy (B). Quantitative analysis results for MMP13-, RUNX2-, pVEGFR2-, and TNFα/TNF-positive chondrocytes in the tibia cartilage (**C** to **F**), and VEGFA, pVEGFR1, NGF, and TNFα/TNF compare the fluorescence intensity and PGP9.5 area percentages in the synovium of mouse knee joints (**G** to **K**) ($n = 3$). Statistical analyses were conducted using one-way ANOVA followed by the Dunnett multiple comparisons test (*$P < 0.05$, **$P < 0.01$, ***$P < 0.001$, and ****$P < 0.0001$). Comparisons were made between groups with or without Nano-PAZII treatment in mice with PMM. Samples were costained with 4′,6-diamidino-2-phenylindole (DAPI) stains to visualize nuclei (blue). Scale bars, 100 μm. FI, fluorescence intensity; a.u., arbitrary units.

Nano-PAZII inhibits VEGFR1-dependent activation of DRG sensory neurons

Peripheral nerve sensitization, a factor contributing to OA pain, is modulated by NGF and VEGFA. These agents jointly play roles in the survival, differentiation, and plasticity of the peripheral nervous system (*15*, *26*). Synovial VEGFA stimulates neuronal nuclei/RNA binding protein fox-1 homolog 3 (NeuN/RBFOX3)-positive sensory neurons in DRG by stimulating NGF/TrkA signaling, a principal pathway that orchestrates the hierarchical development and postnatal synaptic plasticity of nociceptive neurons. Consistent with this model, DRG sensory neurons of mice experiencing OA pain exhibit increased immunofluorescence signals for VEGFA/VEGFR1- and NGF/TrkA-dependent pain-related downstream targets involved in mechanical allodynia or thermal nociception in (Fig. 7). Elevated levels of VEGFA, NGF, and TrkA/NTRK1 in DRG sensory neurons are paralleled by a concomitant increase in the VEGFR1-responsive transient receptor potential vanilloid 1 (TRPV1) protein, the TrkA-responsive calcitonin gene-related protein (CGRP), and phosphorylation of downstream extracellular signal–regulated kinases (ERK1/MAPK3 and ERK2/MAPK1) in OA mice (Fig. 7). However, a single IA injection of Nano-PAZII counteracts these changes while significantly decreasing levels of VEGFA, pVEGFR1, NGF, and TrkA, as

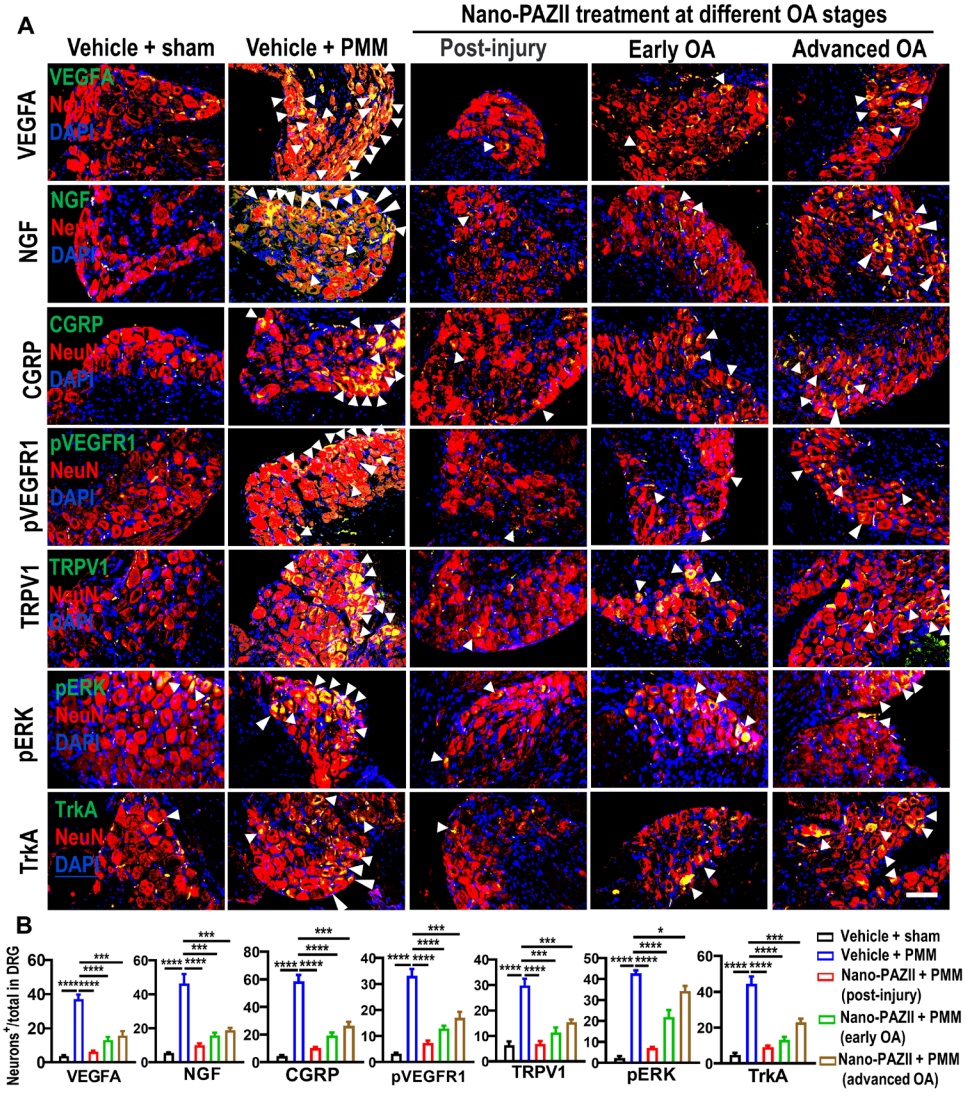

Fig. 7. Molecular effects of Nano-PAZII in DRG sensory neurons associated with peripheral pain sensitivity. IF analysis was performed on histological sections of innervating lumbar DRG (L3/L5) in mice at 16 weeks post-PMM and single Nano-PAZII injection at week 1, 4, or 8 (see Fig. 4B). Microscopic imaging focused on the TrkA-responsive CGRP, which mediates neuroectodermic signaling via downstream effects on extracellular signal–regulated kinases (ERK1/MAPK3 and ERK2/MAPK1), and the VEGFR1-responsive TRPV1 protein, because these markers are associated with mechanical allodynia and thermal nociception. DRG sensory neurons were identified by staining with the neuron-specific nuclear protein NeuN/RBFOX3. (**A**) IF microscopy shows reduced expression of VEGFA, NGF, CGRP, pVEGFR1, TRPV1, pERK, and TrkA/NTRK1 (green; positive cells marked by arrowheads) in sensory neurons identified by NeuN/RBFOX3 as neuron marker (red) by dual label IF microscopy. (**B**) Quantitative analysis shows significantly increased expression of VEGFA, NGF, CGRP, pVEGFR1, TRPV1, pERK, and TrkA/NTRK1 after PMM ($n = 6$). Statistical analyses were conducted using one-way ANOVA followed by the by Dunnett multiple comparisons test (*$P < 0.05$, ***$P < 0.001$, and ****$P < 0.0001$). Comparisons were made between groups with or without Nano-PAZII treatments in mice with PMM. Cells were costained with DAPI to visualize nuclei (blue). Scale bars: 100 μm.

well as the downstream targets CGRP, pERK, and TRPV1 when administered at any of the three stages of disease progression (i.e., post-injury, early OA and advanced OA stages) (Fig. 7). These findings establish the molecular mechanism by which Nano-PAZII blocks mechanical allodynia and thermal nociception as assessed by von Frey filament and hot plate testing (refer to Fig. 4).

Nano-PAZII suppresses microglial cell activity and astrocyte activation in the spinal cord of experimental OA animals

Astrocytes and microglia are critical cellular mediators of chronic pain and sustained inflammation within the spinal cord. In PPM-induced OA mice, there is a notable rise in VEGFA-positive cells, glial fibrillary acidic protein (GFAP)–positive astrocytes, and ionized calcium-binding adaptor molecule 1 (IBA1)-positive microglia in the ipsilateral dorsal horn of their spinal cords (Fig. 8). Nano-PAZII treatment at any of the three stages of OA disease progression significantly reduces the levels of VEGFA, the number of activated astrocytes and microglia cells, as well as VEGFR1 activity (pVEGFR1) in the spinal dorsal horn (Fig. 8). These findings suggest that the VEGFA/VEGFR1 pathway extends its influence beyond angiogenesis, modulating nociceptive synaptic transmission in the spinal dorsal horn (known as central sensitization) and leading to sustained pain symptoms as OA advances.

Nano-PAZII does not induce reward behavior following OA treatment by IA injection

For its potential therapeutic relevance, it is imperative that pain relief by pazopanib does not lead to rewarding behaviors that may be subject to abuse, particularly given the widespread use of opioids in patients with advanced OA and the ongoing opioid crisis (*27*, *28*). We verified that pazopanib does not have abuse liability based on a conditioned place preference (CPP) test. The reference compound, morphine (5 mg/kg), induces a CPP in rats during the testing phase on day 10, because morphine reinforces and conditions animals to prefer drug-paired chambers (*29*, *30*). When animals were treated with pazopanib (either at 30 or 80 mg/kg) during conditioning, sessions they displayed no inclination toward drug versus nondrug chambers on day 10 (Fig. 9). Behavioral analysis of rats during the conditioning sessions highlighted the sedative effects of morphine, with a significant reduction in locomotion evident by the shorter distances covered on day 2. Conversely, pazopanib did not induce significant changes in locomotion (Fig. 9). This leads us to deduce that pazopanib is devoid of opioid-like intrinsic reward mechanisms that reinforce behavioral preferences.

With a focused view toward clinical translation and in anticipation of potential adverse effects when transitioning to clinical trials, localized (IA) injections offer the advantage of substantially mitigating side effects typically associated with immunological and systemic intervention in VEGF signaling. In our assessment, a one-time administration of Nano-PAZII (65 μg per knee joint) presented no toxicological concerns (fig. S6). This finding improves the prospects of implementing Nano-PAZII–based approaches in clinical settings for OA.

DISCUSSION

The symptoms of OA as a disease linked to degeneration of articular cartilage and severe pain are traditionally managed using nonsteroidal anti-inflammatory drugs, acetaminophen, and opioid analgesics (*31*). However, these treatments often come with significant side effects and toxicities (*32*) and primarily address pain as a symptom originating from cartilage damage and concomitant inflammation. What is truly needed in OA treatment are disease-modifying drugs that address joint pain, chronic inflammation, and the deterioration of cartilage (*33*–*36*). Our research indicates that Nano-PAZII holds promise as a DMOAD, given its ability to target OA pain associated with VEGFR1/FLT1 and cartilage degeneration linked to VEGFR2/FLT1 (*15*).

Pazopanib, already approved by the FDA for advanced renal cell carcinoma, functions as a multikinase inhibitor, while it has the potential for systemic pleiotropic effects, such as hepatoxicity upon oral intake (*37*). Therefore, the local administration of pazopanib-loaded nanoparticles through IA injection is a favored route. However, the hydrophobic nature of pazopanib combined with its unfavorable pharmacokinetics affects its bioavailability negatively. Even when used at high concentrations (3 mg/ml) in the knee joint, its therapeutic effects diminish within 3 days (*15*).

To effectively mitigate knee OA pain, twice-weekly IA injections for several months become necessary, posing challenges for clinical settings (*15*). On a more positive note, the advent of nanodelivery systems has considerably enhanced the therapeutic efficacy while minimizing the side effects of anticancer agents (*38*, *39*). This study aimed to address these challenges by introducing a nanoparticle-encapsulated version of pazopanib (Nano-PAZII) developed using biocompatible polymers as a versatile drug release system. We used the biodegradable and biocompatible PEG-*b*-PCL copolymer to ensure well-controlled physicochemical properties for Nano-PAZII. This approach is both scalable and reproducible, essential attributes for clinical applications (*40*, *41*).

Regarding biocompatibility, Nano-PAZII does not affect chondrocyte viability at effective doses (<45 μg/ml, 100 μM) and is well-tolerated upon single IA injection (65 μg per mouse knee joint). This biocompatibility is enhanced by the PEGylation of terminal amines in our nanoparticles, a factor that helps in decreasing toxicity (*42*, *43*). Furthermore, pazopanib is already recognized for its use in treating kidney cancer. Notably, IA injections, even at minimal doses of pazopanib (7.5 μg per knee joint), provided instant pain relief and prevented cartilage degeneration in our PMM model (*15*). Toxicological assessments further confirmed no evidence of systemic toxicity with long-term (twice per week for 12 weeks) (*15*) or after a single IA injection of Nano-PAZII (65 μg per knee joint). These results further assuage potential concerns related to the therapeutic application of either pazopanib or Nano-PAZII.

Nano-PAZII particles have a favorable long shelf life in lyophilized powder form. Before administration, the nanoparticle can be resuspended in aqueous buffers and maintain excellent stability at room temperature, suitable for IA injections. In vitro drug release studies indicate that the breakdown of PEG-*b*-PCL polymeric nanoparticles via hydrolysis of PCL is a gradual process, ensuring consistent drug release with excellent stability for >18 weeks. Our findings provide substantial progress toward the long-term objective to produce nanoparticles that permit sustained local release of pazopanib upon a single IA injection, thereby substantially reducing the potential systemic circulation. Our in vitro studies show that Nano-PAZII continuously releases pazopanib under mildly acidic conditions (pH 3 to pH 5) for more than 16 weeks but not in near neutral conditions (pH 7). Although the precise release mechanism in vivo remains to be further examined, our in vivo studies indicate that Nano-PAZII

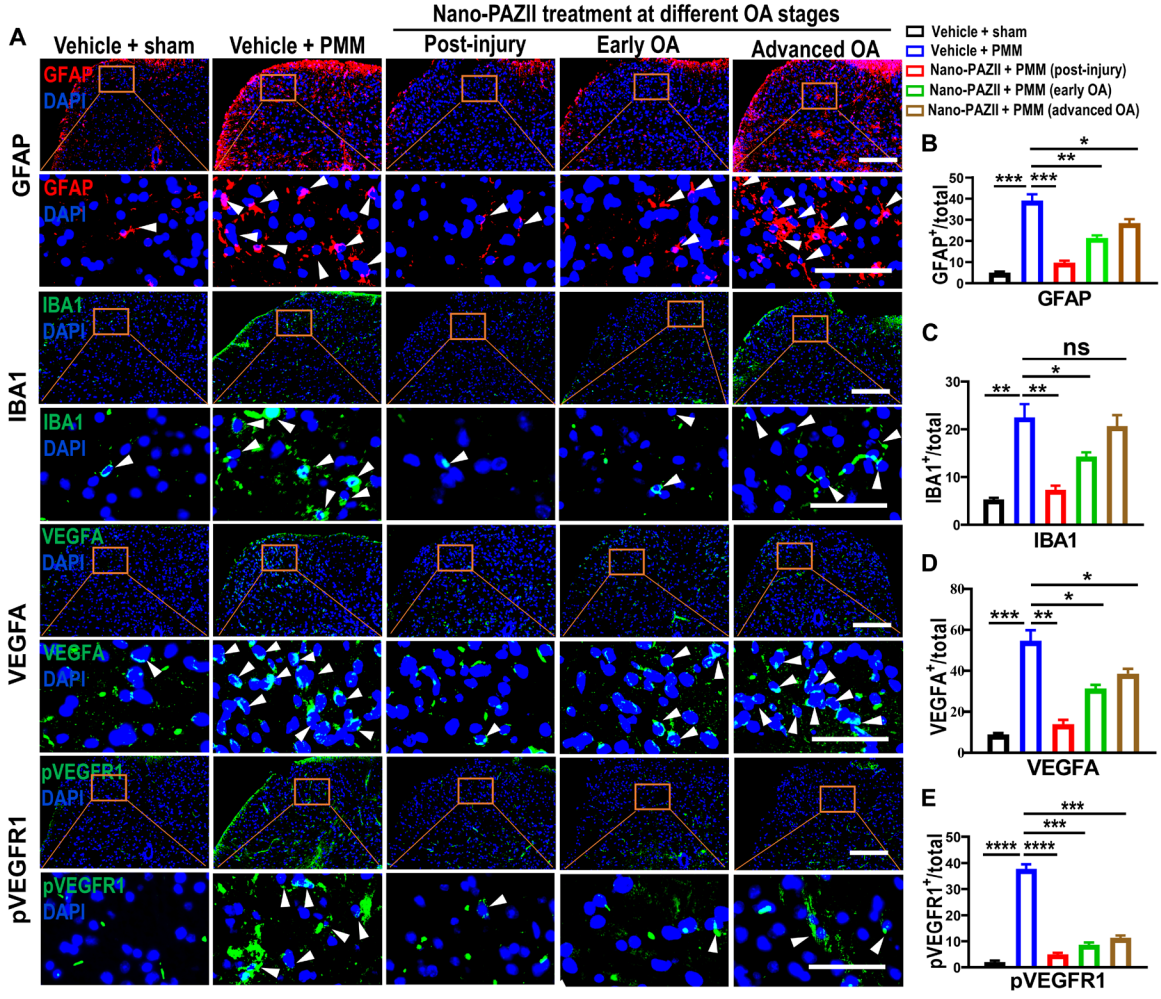

Fig. 8. The effect of a single IA injection of Nano-PAZII in the spinal cord plasticity. Histological sections of spinal cords (L3/L5) were harvested at 16 weeks upon OA induction by PMM and after a single IA injection of Nano-PAZII (or vehicle) at select time points of OA progression after PMM induction (week 1, 4, or 8; see Fig. 4B). Double-label IF microscopy was performed for VEGFA and markers for activation of astrocytes (i.e., *GFAP*) and microglial cells (ionized calcium-binding adaptor molecule 1; *IBA1/AIF1*) at 16 weeks after PMM using IF microscopy. (**A**) Nano-PAZII reduces levels of VEGFA and pVEGFR1, as well as the activity of microglial and astroglial cells in ipsilateral lumbar spinal dorsal horns. Cells positive for expression of the astrocyte marker GFAP (red), the microglia marker IBA1, as well as VEGFA or VEGFR1 (green) are indicated by white arrows (A). (**B** to **E**) Quantitative analyses demonstrate that expression of GFAP, IBA1, VEGFA, and VEGFR1 activation significantly increased after PMM ($n = 3$). Statistical analysis was conducted using one-way ANOVA followed by the Tukey-Kramer test (*$P < 0.05$, **$P < 0.01$, ***$P < 0.001$, and ****$P < 0.0001$). Comparisons were made between groups with or without Nano-PAZII treatment in mice that underwent PMM. Nuclei were visualized with DAPI staining (blue). Scale bars, 100 μm. ns, not significant.

(after a single IA injection) has sustained bioactivity compared to unloaded nanoparticles. The latter suggests that pazopanib is released in vivo in sufficient quantities to have beneficial biological effects. One possible explanation of the apparent bioavailability of Nano-PAZII in vivo at near neutral pH is that interactions with inflammation-related cells (e.g., macrophages) and/or the pericellular matrix compartment of the synovium may perhaps alter the local pH (*44*), and the development of a more acidic microenvironment due to lactate accumulation during OA progression facilitates pazopanib release (*45*–*47*). Future studies will need to resolve the potential benefits of nanoparticles that are engineered to allow the pH-dependent release of pazopanib at near-neutral pH (pH 6 to pH 8) in vitro and what mechanisms would support the controlled release of pazopanib in synovial fluid within the same neutral physiological pH range in vivo.

Extrapolation of our zero-order kinetics results for Nano-PAZII (obtained at low pH) in vitro suggests that the release of pazopanib (at physiological neutral pH) in vivo may occur mainly through diffusion-controlled zero-order kinetics. The latter would be favorable for clinical translation, because the release of pazopanib would be independent of the compound concentration and occurs with minimal burst release. Small molecules and biomacromolecules can be rapidly cleared through the lymphatic system after IA injection (*48*). Given that the diameter of Nano-PAZII spans between 200 and 1000 nm, it is plausible that these particles may be able to penetrate the synovium or deeper cartilage upon degradation to subparticles that would potentially be smaller than the cartilage meshwork size (−60 nm) (*49*). Nano-PAZII's formulation is innovative, with the nanoparticle's size and pazopanib retention properties designed to minimize clearance through the lymphatic system, potentially

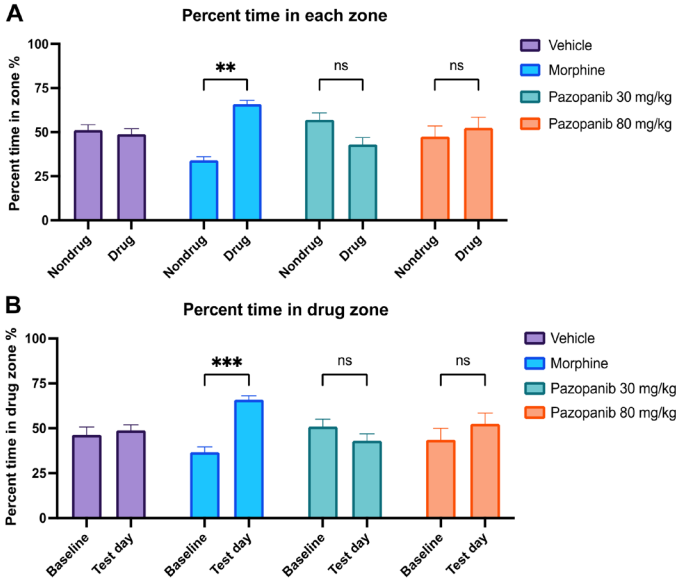

Fig. 9. Drug abuse liability (rewarding properties) for pazopanib in a rat model for CPP. Rewarding properties for the chronic use of pazopanib drug was evaluated by place preference tests by exposing rats to a known addictive drug (morphine) or two different doses of pazopanib (30 or 80 mg/kg). Dwelling time was compared (expressed as a percentage) in a nondrug versus drug chamber at day 10 (**A**) or comparing day 10 with the drug to baseline at day 0 ($n = 8$) (**B**). Statistical analysis was performed using two-way ANOVA followed by Sidak's multiple comparisons test. Data are presented as means ± SEM (**$P < 0.001$ and ***$P < 0.0001$).

improving pazopanib's bioavailability within the synovial cavity. This, in turn, might enhance the bioavailability of pazopanib within the synovial cavity, thus facilitating the efficacy of pazopanib in promoting cartilage homeostasis and diminishing chronic pain.

One noteworthy finding is that a single IA injection of Nano-PAZII introduces considerable improvements in joint pain in mouse OA models (i.e., pain relief for >16 weeks in PMM-OA and >5 weeks in MIA-induced OA), consistent with results on drug release in vitro. Furthermore, it seems that the controlled release of pazopanib via Nano-PAZII considerably enhances pain outcomes by ensuring sustained bioavailability in the joint space. Determining whether the particles localize within synovium or cartilage tissues demands more extensive research, potentially using fluorophore-assisted microscopy studies on Nano-PAZII formulations tailored for clinical use in patients.

In surgical and nonsurgical murine OA models, Nano-PAZII not only addresses OA pain but also suppresses cartilage degeneration, synovial neovascularization, sensory neuron stimulation, and inflammation-associated expression in synovium. Its role in targeting VEGFR1 and VEGFR2 makes it a promising DMOAD candidate. A single IA injection of Nano-PAZII results in notable rapid and long-lasting improvements in joint pain using two distinct surgical and nonsurgical models for murine OA (i.e., PMM- and MIA-induced OA) in vivo. Beyond addressing OA pain which is the most compelling symptom, Nano-PAZII not only suppresses (i) traumatic joint injury–induced cartilage degeneration, (ii) synovial neovascularization, and the increased distribution of sensory neurons in synovium but also (iii) reduces DRG sensory neuronal plasticity, as well as (iv) minimizes activation of spinal glial cells, including microglial cells and astrocytes, thereby preventing central sensitization via nociceptive synaptic transmission in the spinal dorsal horn. Mechanistically, Nano-PAZII simultaneously prevents the inflammation-associated expression of VEGFR1- or VEFGR2-responsive genes linked to cartilage degeneration in chondrocytes, pain-associated mediators in synoviocytes, and relevant pain markers in DRG sensory neurons. Collectively, our study indicates that Nano-PAZII, by simultaneously targets both either VEGFR1 and/or VEGFR2, is an ideal DMOAD candidate with potential benefits in both ameliorating OA joint pain and attenuating cartilage loss in degenerating knee joints. Moreover, the active ingredient pazopanib lacks opioid-like rewarding properties, thus minimizing the risk of drug dependency.

Several OA symptoms in patients, including pain, are attributed to neovascularization and subsequent sensory innervation (*50*). In line with the requirement for VEGFR1/VEGFR2 signaling in mouse models of angiogenesis (*51*, *52*) and ovarian cancer (*53*), we observed that pazopanib inhibits synovial neovascularization and osteophyte formation in our preclinical OA models. Hence, Nano-PAZII could help mitigate OA pain partially by inhibiting the effects of VEGFR2 on synovial blood vessels and osteophyte formation.

The transition from asymptomatic to painful OA occurs independently of joint pathology in humans and in animal models (*8*, *26*, *54*). We and other group identified DRG sensory neuronal overexpression of NGF and its cognate receptor TrkA (NTRK1) as critical determinants in the pain transmission by facilitating axonal outgrowth (*26*, *55*). Activation of VEGFR1 (but not VEGFR2) effectively stimulates the NGF/TrkA signaling pathways in peripheral joint tissues and DRG sensory neurons (*15*). NGF/TrkA signaling becomes activated in DRG after retrograde transport of VEGFA attributed to increased levels of VEGFR1-expressing nerve terminals in OA synovium (*14*). Consequently, Nano-PAZII may block knee OA joint pain through its impact on both peripheral and central pain sensitization by (i) significantly reducing NGF/TrkA signaling pathways in the knee joint and DRG sensory neurons; (ii) inhibiting the increased distribution of sensory neurons in the knee joint synovium; and (iii) decreasing the activation of astroglial and microglial cells in the spinal cord.

Nano-PAZII is a small molecule encapsulated in a relatively stable and biocompatible nanoparticle. Using murine preclinical OA models, Nano-PAZII shows encouraging drug efficacy that compares favorably with other published treatments, including hyaluronic acid and steroids (*56*), gelatin hydrogels with eicosatetraenoic acid (*57*). Our study advances the field by showing that nanoparticle-based delivery of pazopanib prolongs OA pain relief by significantly prolonging the apparent bioavailability and efficacy of pazopanib, presumably by sustaining drug release in synovial fluid.

One limitation of the present work is that the precise functions of VEGFR1 in the induction and maintenance of persistent OA pain, particularly via effects in the parasympathetic nervous system and astrocytes (of the central nervous system), remain elusive. Addressing the latter will require extensive studies with transgenic and/or knockout mouse models, which would involve conditional global- and tissue-specific ablation of the *VEGFR1* gene during OA-induced pain sensitization at the peripheral and central levels. Electrophysiologic data and brain imaging would be essential to

definitively determine the impacts of Nano-PAZII on central pain pathways. In the same vein, while analgesic effects are suggested from the antihyperalgesia effects we observed, future work is needed to extend the assays to include limb use and affective state measures that corroborate the pain-alleviating effects, such as gait analysis. This would ensure that a important role for VEGFR1 in pain and VEGFR2 in cartilage degeneration can be further addressed to define the full spectrum of pazopanib treatment effects in OA. On another note, a single IA injection of Nano-PAZII proves effective when it is administrated at post-injury or early OA pain stages. However, only partial cartilage preservation was achieved by a single IA Nano-PAZII injection when the treatment started at the advanced OA stage. The preservation of cartilage does not match up to treatment regimens initiated at the onset of joint injury. Exploring cotreatments with mesenchymal stem cells might enhance treatment of advanced OA, particularly to address challenges like the lack of cellularity (e.g., worn-out cartilage) in our future studies. Third, a single IA injection of Nano-PAZII has been shown to relieve PMM-induced OA pain for 16 weeks. However, we lack direct evidence showing that Nano-PAZII significantly improves the retention time of pazopanib in the joint capsule. In subsequent research, we plan to track nanoparticles in the joints by adding a fluorophore in the nanoparticles. Furthermore, our studies are qualified by the technical limitation that we cannot yet model the physiologically relevant release of pazopanib from Nano-PAZII under near neutral conditions (at pH = 7), because drug release in vitro is only robust under mildly acidic conditions (pH = 3 to pH = 5). Formally, we have not yet been able to demonstrate specifically how pazopanib concentrations released from Nano-PAZII particles affect the biological properties of human chondrocyte and FLSs. We have extrapolated the consequences of pazopanib release in experiments with these cell types by testing unencapsulated pazopanib without nanoparticles to arrive at the interpretation that Nano-PAZII may block IL-1β/IL1B-related inflammatory events in both chondrocytes and FLSs.

In conclusion, the key finding of this study is that a single IA injection of Nano-PAZII has beneficial effects at different stages of OA disease progression by rapidly reducing knee joint pain, with sustained analgesic effects and marked suppression of cartilage degeneration for months. Furthermore, Nano-PAZII does not affect opioid-related addictive reward behaviors in mice. These properties collectively suggest that Nano-PAZII has potential as a novel DMOAD, providing a promising therapeutic strategy for OA pain treatment and management.

MATERIALS AND METHODS

Study design

This study was performed to evaluate the efficacy of a single IA injection nanoparticle-based sustained delivery of the VEGFR inhibitor pazopanib (Nano-PAZII) upon reversal of OA symptoms in different stages of experimental OA. This objective was addressed by (i) developing a nanoparticle-based formulation of the FDA-approved kinase inhibitor pazopanib (Nano-PAZII) that targets both VEGFR1 and VEGFR2, (ii) studying the effect of a single IA injection of Nano-PAZII in two distinct rodent OA models involving either surgical (PMM) or nonsurgical induction (with MIA), (iii) delineating the altered VEGF/VEGFR signaling changes in knee joints, DRG, and spinal cord by immunofluorescence microscopy, (iv) showing that there is no reward behavior and signs of toxicity upon OA treatment by IA injection of Nano-PAZII. The investigators determined the sample size according to a previous experimental experience. The exact number (n) of tissue samples or cell samples used in each experiment is indicated in the respective figure legends. For in vivo experiments, data from animals that died or had severe health problems during the experiments were excluded. Samples were assigned randomly to the experimental and control groups. Animal or sample allocation and data acquisition in vivo or in vitro were performed in a blinded manner. The investigators were not blinded during data analysis.

Preparation of pazopanib-loaded PEG-*b*-PCL nanoparticles

Pazopanib (molecular mass: 437.517 g/mol; LC Laboratories, MA, USA) (molecular mass: 437.517 g/mol) was encapsulated in PEG-*b*-PCL (Mw 5k-*b*-6.5k, Polymer Source Inc., Quebec, Canada) based nanoparticles that were generated using the FNP method in a custom-made multi-inlet vortex mixer (*22*). One of the four inlet streams (stream 1) contained PEG-*b*-PCL (0.25 mg/ml) and pazopanib (0.25 mg/ml) dissolved in DMSO (Sigma-Aldrich, St. Louis, MO). The other three inlet streams contained deionized water as antisolvent to precipitate the polymer and the drug. The flow rate of streams 1 and 2 was 6 ml/min, while the flow rate of streams 3 and 4 was 54 ml/min (i.e., volumetric flow rate ratio of organic versus aqueous streams was 1:19). The nanoparticle suspension was collected into a beaker containing leucine solution [with leucine (6 μg/ml) in deionized water] under stirring at a 1:1 (v/v) ratio. The mixture was then dialyzed against leucine-deionized water solution (6 μg/ml) using a cellulose dialysis membrane (molecular weight cutoff: 3.5 kDa) for 48 hours to remove DMSO. The solution for dialysis was changed every 2 to 4 hours. Following dialysis, the nanosuspension was freeze-dried in a bench-top freeze-dryer (Labconco, FreeZone 1 Liter Console Freeze Dry Systems, Kansas City, MO) at a vacuum pressure of 0.08 mBar and −108°C for 72 hours to produce stable solid powder. For dosing of animals, nanoparticles were resuspended in PBS buffer solution by sonication for 30 min at a drug concentration of 6.5 mg/ml.

Nanoparticle characterization

Nanoparticle size distributions after FNP and resuspended in PBS buffer were measured by using DLS (Malvern, Cambridge, UK). The particle sizes were reported as the intensity-weighted diameter.

Drug loading (DL) and drug encapsulation efficiency (EF) are defined as follows

$$\mathrm{DL}\ (\%) = \frac{\text{Amount of pazopanib encapsulated in nanoparticles}}{\text{Total weight of nanoparticles}} \times 100\%$$

$$\mathrm{EF}\ (\%) = \frac{\text{Amount of pazopanib encapsulated in nanoparticles}}{\text{Feeding weight of pazopanib}} \times 100\%$$

To experimentally quantify DL and EE values, the dried powder was redissolved in DMSO at a concentration of 1 mg/ml. The amount of pazopanib in the nanoparticles was quantified using a high-performance liquid chromatography (HPLC) system (Shimadzu Scientific Instruments, Columbia, MD) by measuring absorbance at a wavelength of 270 nm. A Hypersil Gold C18 column (2.1 mm by 50 mm, 5 μm; Thermo Fisher Scientific) was used for chromatographic separation, and injection volume to the column was 10 μl. Elution was performed at a flow rate of 0.5 ml/min using a solvent gradient in the

mobile phase that evolved from 5 to 95% organic phase (consisting of 95% acetonitrile/0.1% formic acid) in 7 min.

In vitro drug release from nanoparticles

In vitro drug release studies were performed to understand the diffusion-controlled release of pazopanib from the nanoparticles. The technical design of these experiments was modified to overcome several inherent technical limitations that deviate from physiologically preferred conditions. The diffusion rate of pazopanib is expected to be very slow in aqueous buffer at neutral pH due to the extremely low aqueous solubility of pazopanib and the low degradation rate of the PCL polymer. Without experimental modifications, release of pazopanib in vitro would remain below the detection limit of the HPLC. Drug release was tested in an acidic environment (pH 3 or pH 5), because the hydrolytic degradation of PCL is highly dependent on pH (*58*), and protonation of the carbonyl group in PCL accelerates its degradation rate. This degradation process yields water-soluble products that further reduce the local pH (*59*, *60*). Therefore, we tested in vitro drug release at lower pH to understand the biomaterial properties.

Dried nanoparticle powder was resuspended at pazopanib concentration (0.5 mg/ml) to monitor the drug release in acetate buffer at pH = 3 and pH = 5. The custom-made setup consists of two glass chambers separated by a cellulose membrane (molecular weight cutoff: 3.5 kDa) and was incubated at 37°C to monitor drug release. The bottom chamber contained the nanoparticle suspension, and the top chamber contained the release buffer. The samples were collected from the top chamber and replaced with fresh buffer at predetermined time points. The samples collected from pH = 3 buffer was directly quantified using the HPLC without any further modification. To improve the accuracy, the release samples collected from pH = 5 buffer underwent further drying using lyophilization. The dried powder was redissolved in deionized water with less volume to produce a solution with concentrated pazopanib, which was then quantified using HPLC as described above.

The drug release profile was fitted for zero-order release kinetics, first-order release kinetics, or Higuchi square root of time models. The zero-order release kinetics provided the most optimal data fit. The parameters are as follows

$$C_0 - C_t = K_0 t$$

where C_0 is the concentration of drug release at $t = 0$; C_t is the concentration of drug release at time t; K_0 is the zero-order rate constant; t is the time. The calculated value for pazopanib release from the PEG-*b*-PCL nanoparticles is $K_0 = 4.99 \frac{\text{mol}}{L\ s}$

Cell culture

Human primary chondrocytes derived from normal articular cartilage were purchased from Cell Applications (San Diego, CA, USA) and cultured in chondrocyte growth medium (Cell Applications catalog no. 411-500) (*14*). Chondrocytes were used at first or second passage for all experiments to ensure retention of the proper cell phenotype. FLSs derived from normal synovial tissue were purchased from Cell Applications (San Diego, CA, USA) and cultured in FLS growth medium (Cell Applications catalog no. 415-500). Both chondrocytes and FLSs were maintained in a humidified incubator at 37°C with 5% CO_2.

LDH release assay

Chondrocytes and FLSs were treated with pazopanib or Nano-PAZII with different concentrations for 2 hours, followed by stimulation with interleukin-1β (IL-1β)/IL1B (10 ng/ml) for 16 hours. After the indicated treatments, culture media for all conditions were collected and subjected to the LDH Cytotoxicity Assay kit (Cell Biolabs Inc., CBA-241) according to the manufacturer's instructions. The absorbance at 450 nm was measured using a microplate spectrophotometer (SpectraMax iD3; Molecular Devices LLC., San Jose, CA, USA). The relative LDH release levels were expressed as fold changes relative to untreated control cells.

Quantitative real-time PCR

The chondrocytes and FLSs were pretreated with pazopanib (2.25 μg/ml) for 2 hours and then stimulated with VEGFA (100 ng/ml) or IL-1β/IL1B (10 ng/ml) for 6 hours. Total mRNA was extracted with TRIzol (Invitrogen Life Technologies, CA, USA), and cDNA was synthesized using a cDNA synthesis kit (iScript cDNA Synthesis Kit, Bio-Rad) using 1 μg of total RNA according to the manufacturer's instructions. Analyses by quantitative reverse transcription polymerase chain reaction (qRT-PCR) were conducted using a Bio-Rad CFX Connect system (Bio-Rad Laboratories, CA) and the SYBR Green method (Bio-Rad Laboratories). We obtained a threshold cycle (C_t) value and determined relative mRNA expression by the $\Delta\Delta C_t$ method using the expression of human glyceraldehyde phosphate dehydrogenase mRNA as internal control. All qRT-PCR reactions were performed in triplicate using sequence-specific forward and reverse primer sequences (table S1).

Generation of PMM-induced and MIA-induced OA mouse models and Nano-PAZII treatment

Female C57BL/6 mice were procured from the Jackson Laboratory (Bar Harbor, ME) and maintained in the animal care facility of the Jesse Brown Veterans Affairs Medical Center (JBVAMC), Chicago in a temperature-controlled room (25° ± 5°C) with a 12-hour light-dark cycle. All animal studies were duly approved by the Institutional Animal Care and Use Committee (IACUC) of the University of Illinois at Chicago and JBVAMC (see schematic representation of the protocol in Fig. 4).

OA was induced in 12-week-old mice by PMM according to established methods (*14*, *15*). Briefly, mice were pretreated with buprenorphine (0.1 mg/kg) subcutaneously and then anesthetized with intraperitoneal injection of ketamine (100 mg/kg) and xylazine (5 mg/kg). Adequate anesthesia was confirmed by careful pinch tests, and mice were under anesthesia for less than 5 min. To perform PMM, which destabilizes the ligaments, a micro scalpel was used at a depth of 0.5 mm to remove the meniscus at the midline. Sham surgery was performed by following the same procedures except for the meniscectomy. PMM and sham surgery were performed under anesthesia and sterile conditions using a medial parapatellar approach. Experiments continued for 16 weeks after PMM based on the time course analysis of OA pathology at these time points, day 5 (the post-injury stage), week 4 (early OA), or week 8 (advanced OA) after surgery.

MIA-induced arthritis was performed according to previously published (*61*) protocols. Briefly, MIA (0.5 mg per knee; 5 μl, I2512, Sigma-Aldrich) was applied by IA injection into the left knee joint cavity of naive mice. Identical amounts of sterile saline served as vehicle controls.

Nano-PAZII treatments (6.5 mg/ml, 5 or 10 μl) were done by injection of drugs into the left knee joint cavity of mice with PMM at day 5 (the post-injury stage), week 4 (treatment for early OA), or week 8 (treatment for advanced OA) after surgery. Nanoparticles without pazopanib loading (vehicle) in a volume of 5 or 10 μl served as negative controls for mice with PMM or sham surgery. We also included a single IA injection of pazopanib group (7.5 μg per knee, 1.5 mg/ml, 5 μl) in mice with PMM at day 5 (the post-injury stage). On the basis of our previous study, a higher concentration of pazopanib (3 mg/ml) did not further improve the pain condition, and we selected 1.5 mg/ml concentration for IA injection of pazopanib for the study (*15*).

In the MIA-induced OA mouse model, Nano-PAZII treatments (6.5 mg/ml, 10 μl) were performed by IA injection of drugs into the left knee joint cavity at day 3 (the post-injury stage), day 7 (treatment for early OA), or day 14 (treatment for advanced OA) after MIA injection. Nanoparticles without pazopanib loading (vehicle) in a volume of 10 μl served as controls.

CPP test for examination of physiological reward behavior

Standard CPP testing in rats was performed to examine whether pazopanib is devoid of potential addictive (reward) properties. This model measures the reinforcing properties of a drug in the absence of the drug itself. We tested for abuse potential following intraperitoneal administration, exposing the animals to far greater drug concentrations than would be expected from IA administration as a robust test of abuse potential. Male Sprague-Dawley rats (200 to 250 g, 8 to 9 weeks old at the beginning of the experiments) were procured from Charles River Labs. Rats were housed on a 12-hour light/dark cycle (lights on 7:00 a.m.) with free access to food and water. The animal protocol was approved by Mellor Discovery IACUC, and rats were assigned randomly to treatment groups (table S2). The reference compound (morphine at 5 mg/kg) was used as a positive control and induced a CPP in rats during the testing phase on day 10. Pazopanib was administered at two different doses (30 or 80 mg/kg) for the addictive test.

Treated rats were examined using a CPP apparatus (Med Associates, Fairfax, VT, USA), which measures place preference by monitoring the movement of mice into one of two compartments (black or white) via a manual door. The CPP device is controlled by MED-PC IV software (Med Associates, Fairfax, VT, USA), and preference testing began on day 1 with 15 min of acclimatization to the apparatus. On day 1 (preconditioning test), mice were allowed to freely explore the whole apparatus for 20 min. Time spent in each chamber was recorded for baseline purposes. Using a biased design, the chamber in which any one animal spent the most time was designated as the "preferred chamber" and assigned as the "vehicle chamber." The "least preferred" chamber was assigned as the "drug chamber." If rats failed to prefer one chamber, then vehicle and drug chambers were assigned randomly. After habituation, rats were injected with the compounds or vehicle (table S2). During the conditioning days (days 2 to 9), rats were dosed orally with pazopanib (30 or 80 mg/kg) or its vehicle (days 2, 4, 6, and 8) or saline (days 2, 4, 6, 8, and 10), and 30 min later, animals were dosed subcutaneously at 1 ml/kg with morphine or saline (table S2) and immediately placed into the drug chamber for 30 min. Rats were placed into chambers and allowed to move freely between the two distinct compartments for 30 min on day 10. Time spent in each chamber was recorded. The study measured the time spent in the drug-paired chamber versus the vehicle-paired chamber during the test session on day 10. Quantitative values that were recorded during drug conditioning sessions (days 2, 4, 6, and 8) and on the testing session (day 10) include absolute duration in the chamber (in seconds), relative duration (as a percentage of the testing session), and locomotor activity (distance traveled in centimeters).

Longitudinal behavioral pain measurements

Longitudinal behavioral pain measurements, including mechanical allodynia (von Frey filament tests) and hot thermal sensitivity assay (hot plate tests), were performed at baseline (before OA induction) and thereafter weekly for 16 weeks (PMM model) or 5 weeks (MIA model). Mice were acclimated to the testing environment and equipment for 15 min before each time point.

Mechanical allodynia assays (von Frey testing) were measured by placing animals on a perforated metal "grid" floor (with 5-mm-diameter holes placed 7 mm apart) within small plexiglass cubicles (9 cm by 5 cm by 5 cm high). Seven calibrated von Frey fibers (Stoelting touch Test Sensory Evaluator Kit) were applied in sequence to the plantar surface of the hind paw until the fiber began to bow and then held for 2 to 3 s by the up-down method (*15*, *62*, *63*). We use the following range of filaments labeled by force and handle number in parenthesis; 0.04 g (2.44), 0.07 g (2.83), 0.16 g (3.22), 0.4 g (3.61), 1.0 g (4.08), 2.0 g (4.31), and 6.0 g (4.74). For the first trial, use the 3.61 (0.4 g), filament for mice. The threshold force required to elicit the withdrawal of the paw was determined. A brisk lifting of the foot was recorded as a positive response. If no response was observed, then the filament with the next highest force was applied, while the filament with the next lowest force was applied after a positive response (*14*, *15*). Behavioral analyses were performed in a blinded manner.

Hot thermal sensitivity assays (hot plate testing) measured the temperature sensitivity of the hind paw using a "Hotplate Analgesia Meter" (Columbus Instruments, Columbus, USA). Before the experiment, the top plate was cleaned with alcohol, the hot plate was set to 55°C, and the plate was turned on for at least 30 min to allow stabilization at 55°C. Mice were placed into the hot plate enclosure, and the timing was recorded when any of the following behavioral events occurred: licking the hind paw (even once), shaking the hind paw in the air, and jumping. A cutoff latency of 20 s was used to prevent tissue damage (*14*, *15*). Behavioral analyses were performed in a blinded manner.

Histopathology and Immunofluorescence

Histopathological and immunohistochemical analyses were performed as we previously described (*14*, *15*, *26*). Gross knee joint pathology was examined using standard procedures described previously (*14*, *15*). At 16 weeks post-PMM or postsham surgery, animals were terminally anesthetized and preperfused with 4% paraformaldehyde (PFA) in PBS (pH 7.4). Knee joint samples were then further fixed in 4% PFA/PBS (pH 7.4) for 48 hours at 4°C, decalcified for 14 days in chelation buffer (0.5 M EDTA (pH 8.0), Invitrogen, AM9262) at 4°C. Entire knee joints were serially sectioned (5 μm) in the sagittal or coronal plane for histological analysis and immunofluorescence microscopy. Two sections within every consecutive six sections in the entire section set for each knee were stained with Safranin O and fast green, hematoxylin and eosin (H&E), and Alcian blue/hematoxylin and orange G (AB/H&OG) for morphologic analysis (*64*, *65*). The severity of

OA-like phenotypes was analyzed by two blinded observers who scored cartilage degeneration (using OARSI scoring), cartilage thickness, synovitis, osteophyte formation, and neovascularization in three-level parallel sections of the joint specimens (*14*, *15*). The average articular cartilage thickness of the medial tibia plateau was quantified by tracing the Safranin O–positive staining using the ImageJ software (National Institutes of Health, Bethesda, MD, USA) (*66*). Changes in synovial tissue were semiquantified by the number of synovial lining layers (*66*). The osteophyte formation was evaluated semiquantitatively based on both size and maturity of osteophytes using AB/H&OG staining (*64*, *65*). In addition, the ipsilateral lumbar (L3-5) DRG and spinal cord were isolated and postfixed with 4% PFA/PBS (pH 7.4) for 48 hours and then processed for paraffin embedding and sectioning.

Sections were incubated overnight at 4°C in primary antibodies against pVEGFR1 (1:100; Invitrogen, PA5-99362), pVEGFR2 (1:100; Invitrogen, PA5-105765), VEGFA (1:500; Abcam, ab185238), NGF (1:500; Abcam, ab52918), IBA1 (1:100; Abcam, ab178846), NeuN (1:500; Abcam, ab104224), pERK (1:200; Invitrogen, PA5-99447), CGRP (1:200; Abcam, ab81887), TRPV1 (1:200; Abcam, ab6166), RUNX2 (1:100; Abcam, ab192256), PGP9.5 (1:200; Abcam, ab104404), TNFα (1:500; Abcam, ab1793), TrkA (1:100; Invitrogen, MA-32123), MMP-13 (1:500; Sigma-Aldrich, MAB13424), CD31 (1:100; Abcam, ab182981), and GFAP (1:200; Sigma-Aldrich, HPA056030). After rinsing three times with PBS, sections were incubated in Alexa Fluor 546 goat anti-rabbit immunoglobulin G (IgG; 1:500; Invitrogen, A-11035) or goat anti-mouse Alexa Fluor 488 IgG (1:500; Invitrogen, A-11029) for 2 hour. Sections were rinsed with PBS and attached to slides by mounting medium with 4′,6-diamidino-2-phenylindole (DAPI; SouthernBiotech) and covered with coverslips. Fluorescent images were obtained with a Nikon Eclipse NiE upright microscope (Nikon Instruments Inc., Melville, NY) at the same exposure setting and associated software.

Toxicological evaluation of chronic use of IA drug administration

Mice received a single IA injection of Nano-PAZII (6.5 mg/ml, 10 μl) or vehicle (nanoparticles without pazopanib, 10 μl) at day 5 (post-injury stage) after PMM. Body weights of all the animals were measured every week, and behavioral changes were observed. After drug or vehicle treatments for 16 weeks, animals were euthanized, and vital organs (e.g., heart, kidney, liver, and pancreas) were isolated. Histopathological studies were performed on these vital organs using H&E staining. Briefly, the specimens were fixed in 10% formalin and processed. After the tissue was embedded in paraffin and sectioned at 5-μm thickness, sections were stained with H&E according to the procedure. Photomicrographs were taken with a Nikon light microscope (×200 magnification), and semiquantitative toxicological evaluation was performed by examining structural changes in tissue architecture based on H&E staining as described previously (*14*, *15*). Each organ tissue resulted in 10 images. For a semiquantitative comparison of the structural changes, abnormalities in the tissue sections were graded from 0 (normal structure) to 3 (severe pathological changes).

Statistical analysis

Data are presented as the mean ± SEM, as indicated in the figure legends. Unpaired Student's *t* tests were used to determine *P* values for comparisons between two groups, while one-way or two-way analysis of variance (ANOVA) with Tukey-Kramer or Dunnett or Sidak's multiple comparisons test was used for comparisons among more than two group. For cell culture experiments, observations were repeated independently at least three times, and data from representative experiments are presented. Statistical analyses were performed using GraphPad Prism 10 software (GraphPad Software, San Diego CA, USA) with $P < 0.05$ considered statistically significant.

Supplementary Materials

This PDF file includes:

Figs. S1 to S6

Tables S1 and S2

REFERENCES AND NOTES

1. N. Fine, S. Lively, C. A. Séguin, A. V. Perruccio, M. Kapoor, R. Rampersaud, Intervertebral disc degeneration and osteoarthritis: A common molecular disease spectrum. *Nat. Rev. Rheumatol.* **19**, 136–152 (2023).
2. A. Latourte, M. Kloppenburg, P. Richette, Emerging pharmaceutical therapies for osteoarthritis. *Nat. Rev. Rheumatol.* **16**, 673–688 (2020).
3. S. Onuora, Single-cell-based platform maps response to candidate DMOADs. *Nat. Rev. Rheumatol.* **18**, 672 (2022).
4. J. S. Rockel, M. Kapoor, Understanding synovial cell diversity in post-traumatic OA. *Nat. Rev. Rheumatol.* **19**, 4–5 (2023).
5. I. Bernabei, A. So, N. Busso, S. Nasi, Cartilage calcification in osteoarthritis: Mechanisms and clinical relevance. *Nat. Rev. Rheumatol.* **19**, 10–27 (2023).
6. A. Eccleston, Cartilage regeneration for osteoarthritis. *Nat. Rev. Drug Discov.* **22**, 96 (2023).
7. P. Wojdasiewicz, Ł. A. Poniatowski, D. Szukiewicz, The role of inflammatory and anti-inflammatory cytokines in the pathogenesis of osteoarthritis. *Mediators Inflamm.* **2014**, 561459 (2014).
8. J. L. Hamilton, M. Nagao, B. R. Levine, D. Chen, B. R. Olsen, H. J. Im, Targeting VEGF and its receptors for the treatment of osteoarthritis and associated pain. *J. Bone Miner. Res.* **31**, 911–924 (2016).
9. V. Di Nicola, Degenerative osteoarthritis a reversible chronic disease. *Regen. Ther.* **15**, 149–160 (2020).
10. M. Shibuya, Vascular endothelial growth factor (VEGF) and its receptor (VEGFR) signaling in angiogenesis: A crucial target for anti- and pro-angiogenic therapies. *Genes Cancer* **2**, 1097–1105 (2011).
11. S. Koch, S. Tugues, X. Li, L. Gualandi, L. Claesson-Welsh, Signal transduction by vascular endothelial growth factor receptors. *Biochem. J.* **437**, 169–183 (2012).
12. M. Nagao, J. L. Hamilton, R. Kc, A. D. Berendsen, X. Duan, C. W. Cheong, X. Li, H. J. Im, B. R. Olsen, Vascular endothelial growth factor in cartilage development and osteoarthritis. *Sci. Rep.* **7**, 13027 (2017).
13. V. Das, R. Kc, X. Li, D. Varma, S. Qiu, J. S. Kroin, C. B. Forsyth, A. Keshavarzian, A. J. van Wijnen, T. J. Park, G. S. Stein, I. O-Sullivan, T. P. Burris, H.-J. Im, Pharmacological targeting of the mammalian clock reveals a novel analgesic for osteoarthritis-induced pain. *Gene* **655**, 1–12 (2018).
14. V. Das, R. Kc, X. Li, I. O-Sullivan, A. J. van Wijnen, J. S. Kroin, B. Pytowski, D. T. Applegate, G. Votta-Velis, R. L. Ripper, T. J. Park, H.-J. Im, Blockade of vascular endothelial growth factor receptor-1 (Flt-1), reveals a novel analgesic for osteoarthritis-induced joint pain, reveals a novel analgesic for osteoarthritis-induced joint pain. *Gene Rep.* **11**, 94–100 (2018).
15. K. Ma, G. Singh, J. Wang, I. O-Sullivan, G. Votta-Velis, B. Bruce, A. N. Anbazhagan, A. J. van Wijnen, H.-J. Im, Targeting vascular endothelial growth factor receptors as a therapeutic strategy for osteoarthritis and associated pain. *Int. J. Biol. Sci.* **19**, 675–690 (2023).
16. M. Murata, K. Yudoh, K. Masuko, The potential role of vascular endothelial growth factor (VEGF) in cartilage: How the angiogenic factor could be involved in the pathogenesis of osteoarthritis? *Osteoarthritis Cartilage* **16**, 279–286 (2008).
17. R. Roskoski Jr., Vascular endothelial growth factor (VEGF) and VEGF receptor inhibitors in the treatment of renal cell carcinomas. *Pharmacol. Res.* **120**, 116–132 (2017).
18. M. B. Stephens, A. I. Beutler, F. G. O'Connor, Musculoskeletal injections: A review of the evidence. *Am. Fam. Physician* **78**, 971–976 (2008).
19. E. Ayhan, H. Kesmezacar, I. Akgun, Intraarticular injections (corticosteroid, hyaluronic acid, platelet rich plasma) for the knee osteoarthritis. *World J. Orthop.* **5**, 351–361 (2014).
20. R. M. J. M. van Geel, J. H. Beijnen, J. H. M. Schellens, Concise drug review: Pazopanib and axitinib. *Oncologist* **17**, 1081–1089 (2012).
21. K. G. Csaky, P. U. Dugel, A. J. Pierce, M. A. Fries, D. S. Kelly, R. P. Danis, J. I. Wurzelmann, C. F. Xu, M. Hossain, T. Trivedi, Clinical evaluation of pazopanib eye drops versus ranibizumab intravitreal injections in subjects with neovascular age-related macular degeneration. *Ophthalmology* **122**, 579–588 (2015).

22. H. Shen, S. Hong, R. K. Prud'homme, Y. Liu, Self-assembling process of flash nanoprecipitation in a multi-inlet vortex mixer to produce drug-loaded polymeric nanoparticles. *J. Nanopart. Res.* **13**, 4109–4120 (2011).
23. B. Mukherjee, K. Santra, G. Pattnaik, S. Ghosh, Preparation, characterization and in-vitro evaluation of sustained release protein-loaded nanoparticles based on biodegradable polymers. *Int. J. Nanomedicine* **3**, 487–496 (2008).
24. H. Danafar, S. Davaran, K. Rostamizadeh, H. Valizadeh, M. Hamidi, Biodegradable m-PEG/PCL core-shell micelles: Preparation and characterization as a sustained release formulation for curcumin. *Adv. Pharm. Bull.* **4** (Suppl 2), 501–510 (2014).
25. Y. Liu, K. Kathan, W. Saad, R. K. Prud'homme, Ostwald ripening of beta-carotene nanoparticles. *Phys. Rev. Lett.* **98**, 036102 (2007).
26. I. O-Sullivan, R. Kc, G. Singh, V. Das, K. Ma, X. Li, F. Mwale, G. Votta-Velis, B. Bruce, A. N. Anbazhagan, A. J. van Wijnen, H.-J. Im, Sensory neuron-specific deletion of tropomyosin receptor kinase A (TrkA) in mice abolishes osteoarthritis (OA) pain via NGF/TrkA intervention of peripheral sensitization. *Int. J. Mol. Sci.* **23**, 12076 (2022).
27. L. P. Carter, R. R. Griffiths, Principles of laboratory assessment of drug abuse liability and implications for clinical development. *Drug Alcohol Depend.* **105** (Suppl 1), S14–S25 (2009).
28. W. J. Lynch, K. L. Nicholson, M. E. Dance, R. W. Morgan, P. L. Foley, Animal models of substance abuse and addiction: Implications for science, animal welfare, and society. *Comp. Med.* **60**, 177–188 (2010).
29. L. Kudla, R. Bugno, U. Skupio, L. Wiktorowska, W. Solecki, A. Wojtas, K. Golembiowska, F. Zádor, S. Benyhe, S. Buda, W. Makuch, B. Przewlocka, A. J. Bojarski, R. Przewlocki, Functional characterization of a novel opioid, PZM21, and its effects on the behavioural responses to morphine. *Br. J. Pharmacol.* **176**, 4434–4445 (2019).
30. G. McKendrick, N. M. Graziane, Drug-induced conditioned place preference and its practical use in substance use disorder research. *Front. Behav. Neurosci.* **14**, 582147 (2020).
31. H. Yu, T. Huang, W. W. Lu, L. Tong, D. Chen, Osteoarthritis pain. *Int. J. Mol. Sci.* **23**, 4642 (2022).
32. J. G. Quicke, P. G. Conaghan, N. Corp, G. Peat, Osteoarthritis year in review 2021: Epidemiology & therapy. *Osteoarthr. Cartil.* **30**, 196–206 (2022).
33. S. Grässel, D. Muschter, Recent advances in the treatment of osteoarthritis. *F1000Res.* **9**, 325 (2020).
34. S. Mehta, T. He, A. G. Bajpayee, Recent advances in targeted drug delivery for treatment of osteoarthritis. *Curr. Opin. Rheumatol.* **33**, 94–109 (2021).
35. W. M. Oo, C. Little, V. Duong, D. J. Hunter, The development of disease-modifying therapies for osteoarthritis (DMOADs): The evidence to date. *Drug Des. Devel. Ther.* **15**, 2921–2945 (2021).
36. Y. Wei, L. Yan, L. Luo, T. Gui, B. Jang, A. Amirshaghaghi, T. You, A. Tsourkas, L. Qin, Z. Cheng, Phospholipase A_2 inhibitor-loaded micellar nanoparticles attenuate inflammation and mitigate osteoarthritis progression. *Sci. Adv.* **7**, eabe6374 (2021).
37. B. A. Davidson, A. A. Secord, Profile of pazopanib and its potential in the treatment of epithelial ovarian cancer. *Int. J. Womens Health* **6**, 289–300 (2014).
38. S. Su, P. M. Kang, Recent advances in nanocarrier-assisted therapeutics delivery systems. *Pharmaceutics* **12**, 837 (2020).
39. L. Yan, J. Shen, J. Wang, X. Yang, S. Dong, S. Lu, Nanoparticle-based drug delivery system: A patient-friendly chemotherapy for oncology. *Dose Response* **18**, 1559325820936161 (2020).
40. H. Shen, X. Hu, M. Szymusiak, Z. J. Wang, Y. Liu, Orally administered nanocurcumin to attenuate morphine tolerance: Comparison between negatively charged PLGA and partially and fully PEGylated nanoparticles. *Mol. Pharm.* **10**, 4546–4551 (2013).
41. M. Szymusiak, X. Hu, P. A. Leon Plata, P. Ciupinski, Z. J. Wang, Y. Liu, Bioavailability of curcumin and curcumin glucuronide in the central nervous system of mice after oral delivery of nano-curcumin. *Int. J. Pharm.* **511**, 415–423 (2016).
42. S. Zhu, M. Hong, G. Tang, L. Qian, J. Lin, Y. Jiang, Y. Pei, Partly PEGylated polyamidoamine dendrimer for tumor-selective targeting of doxorubicin: The effects of PEGylation degree and drug conjugation style. *Biomaterials* **31**, 1360–1371 (2010).
43. B. C. Geiger, S. Wang, R. F. Padera Jr., A. J. Grodzinsky, P. T. Hammond, Cartilage-penetrating nanocarriers improve delivery and efficacy of growth factor treatment of osteoarthritis. *Sci. Transl. Med.* **10**, eaat8800 (2018).
44. P. Dainese, H. Mahieu, S. De Mits, R. Wittoek, J. Stautemas, P. Calders, Associations between markers of inflammation and altered pain perception mechanisms in people with knee osteoarthritis: A systematic review. *RMD Open* **9**, e002945 (2023).
45. F. Xiong, Z. Qin, H. Chen, Q. Lan, Z. Wang, N. Lan, Y. Yang, L. Zheng, J. Zhao, D. Kai, pH-responsive and hyaluronic acid-functionalized metal-organic frameworks for therapy of osteoarthritis. *J. Nanobiotechnology* **18**, 139 (2020).
46. X. Wu, X. Fan, R. Crawford, Y. Xiao, I. Prasadam, The metabolic landscape in osteoarthritis. *Aging Dis.* **13**, 1166–1182 (2022).
47. Z. Wang, Y. Zhong, S. He, R. Liang, C. Liao, L. Zheng, J. Zhao, Application of the pH-responsive PCL/PEG-Nar nanofiber membrane in the treatment of osteoarthritis. *Front. Bioeng. Biotechnol.* **10**, 859442 (2022).
48. H. Huang, Z. Lou, S. Zheng, J. Wu, Q. Yao, R. Chen, L. Kou, D. Chen, Intra-articular drug delivery systems for osteoarthritis therapy: Shifting from sustained release to enhancing penetration into cartilage. *Drug Deliv.* **29**, 767–791 (2022).
49. C. Sacchetti, R. Liu-Bryan, A. Magrini, N. Rosato, N. Bottini, M. Bottini, Polyethylene-glycol-modified single-walled carbon nanotubes for intra-articular delivery to chondrocytes. *ACS Nano* **8**, 12280–12291 (2014).
50. P. I. Mapp, D. A. Walsh, Mechanisms and targets of angiogenesis and nerve growth in osteoarthritis. *Nat. Rev. Rheumatol.* **8**, 390–398 (2012).
51. J. I. Greenberg, D. J. Shields, S. G. Barillas, L. M. Acevedo, E. Murphy, J. Huang, L. Scheppke, C. Stockmann, R. S. Johnson, N. Angle, D. A. Cheresh, A role for VEGF as a negative regulator of pericyte function and vessel maturation. *Nature* **456**, 809–813 (2008).
52. T. D. Tailor, G. Hanna, P. S. Yarmolenko, M. R. Dreher, A. S. Betof, A. B. Nixon, I. Spasojevic, M. W. Dewhirst, Effect of pazopanib on tumor microenvironment and liposome delivery. *Mol. Cancer Ther.* **9**, 1798–1808 (2010).
53. W. M. Merritt, A. M. Nick, A. R. Carroll, C. Lu, K. Matsuo, M. Dumble, N. Jennings, S. Zhang, Y. G. Lin, W. A. Spannuth, A. A. Kamat, R. L. Stone, M. M. K. Shahzad, R. L. Coleman, R. Kumar, A. K. Sood, Bridging the gap between cytotoxic and biologic therapy with metronomic topotecan and pazopanib in ovarian cancer. *Mol. Cancer Ther.* **9**, 985–995 (2010).
54. T. L. Vincent, Peripheral pain mechanisms in osteoarthritis. *Pain* **161** (Suppl 1), S138–S146 (2020).
55. P. W. Mantyh, M. Koltzenburg, L. M. Mendell, L. Tive, D. L. Shelton, Antagonism of nerve growth factor-TrkA signaling and the relief of pain. *Anesthesiology* **115**, 189–204 (2011).
56. J. S. Kroin, R. Kc, X. Li, J. L. Hamilton, V. Das, A. J. van Wijnen, O. M. Dall, D. A. Shelly, T. Kenworth, H. J. Im, Intraarticular slow-release triamcinolone acetate reduces allodynia in an experimental mouse knee osteoarthritis model. *Gene* **591**, 1–5 (2016).
57. M. Tsubosaka, S. Kihara, S. Hayashi, J. Nagata, T. Kuwahara, M. Fujita, K. Kikuchi, Y. Takashima, T. Kamenaga, Y. Kuroda, K. Takeuchi, K. Fukuda, K. Takayama, S. Hashimoto, T. Matsumoto, T. Niikura, Y. Tabata, R. Kuroda, Gelatin hydrogels with eicosapentaenoic acid can prevent osteoarthritis progression in vivo in a mouse model. *J. Orthop. Res.* **38**, 2157–2169 (2020).
58. L. N. Woodard, M. A. Grunlan, Hydrolytic degradation and erosion of polyester biomaterials. *ACS Macro Lett.* **7**, 976–982 (2018).
59. P. Grossen, D. Witzigmann, S. Sieber, J. Huwyler, PEG-PCL-based nanomedicines: A biodegradable drug delivery system and its application. *J. Control. Release* **260**, 46–60 (2017).
60. Y. Li, M. Leng, M. Cai, L. Huang, Y. Chen, X. Luo, pH responsive micelles based on copolymers mPEG-PCL-PDEA: The relationship between composition and properties. *Colloids Surf. B Biointerfaces* **154**, 397–407 (2017).
61. H. J. Im, J. S. Kim, X. Li, N. Kotwal, D. R. Sumner, A. J. van Wijnen, F. J. Davis, D. Yan, B. Levine, J. L. Henry, J. Desevré, J. S. Kroin, Alteration of sensory neurons and spinal response to an experimental osteoarthritis pain model. *Arthritis Rheum.* **62**, 2995–3005 (2010).
62. M. J. Piel, J. S. Kroin, H. J. Im, Assessment of knee joint pain in experimental rodent models of osteoarthritis. *Methods Mol. Biol.* **1226**, 175–181 (2015).
63. M. Alves-Simões, Rodent models of knee osteoarthritis for pain research. *Osteoarthr. Cartil.* **30**, 802–814 (2022).
64. J. Li, Y. Wang, D. Chen, R. Liu-Bryan, Oral administration of berberine limits post-traumatic osteoarthritis development and associated pain via AMP-activated protein kinase (AMPK) in mice. *Osteoarthr. Cartil.* **30**, 160–171 (2022).
65. C. B. Little, A. Barai, D. Burkhardt, S. M. Smith, A. J. Fosang, Z. Werb, M. Shah, E. W. Thompson, Matrix metalloproteinase 13-deficient mice are resistant to osteoarthritic cartilage erosion but not chondrocyte hypertrophy or osteophyte development. *Arthritis Rheum.* **60**, 3723–3733 (2009).
66. Y. Wei, L. Luo, T. Gui, F. Yu, L. Yan, L. Yao, L. Zhong, W. Yu, B. Han, J. M. Patel, J. F. Liu, F. Beier, L. S. Levin, C. Nelson, Z. Shao, L. Han, R. L. Mauck, A. Tsourkas, J. Ahn, Z. Cheng, L. Qin, Targeting cartilage EGFR pathway for osteoarthritis treatment. *Sci. Transl. Med.* **13**, eabb3946 (2021).

Acknowledgments: We appreciate all the individuals for participation in this study. **Funding:** This study was supported by NIH R01 (AR077890), DOD (W81XWH-21-1-0549), VA Research Career Scientist Award (IK6BX004477), a Veterans Affairs (VA) Merit Award (I01BX002647), and DOD (W81XWH2210882) to H.-J.I. and Canadian Institute of Health Research (CIHR) (202109PJT-468751-BME-CFAF-48228) to F.M. The views in the manuscript are not official views of the federal government. **Author contributions:** Conceptualization: H.-J.I., K.M., and Y.L. Methodology: H.-J.I., K.M., T.P., J.W., I.O.-S., A.D., S.D., and Y.L. Investigation: K.M., T.P., J.W., I.O.-S., A.D., and S.D. Visualization: K.M., T.P., and J.W. Funding acquisition: H.-J.I. and YL. Project administration: H.-J.I., Y.L., and K.M. Supervision: H.-J.I. and Y.L. Writing—original draft: K.M., T.P., A.J.W., and J.W. Writing—review and editing: H.-J.I., K.M., T.P., J.W., A.J.W., F.M., Z.F., G.V.-V., B.B., and Y.L. **Competing interests:** K.M., Y.L., and H.-J.I. are inventors of a patent application with the title "Nano-formulations of pazopanib, compositions comprising the same, and methods of treating osteoarthritis" by the University of Illinois at Chicago and the United States Department of Veterans Affairs (application #63/208,137, filed on 8 June 2021). The authors declare that they have no other competing interests. **Data and materials availability:** All data needed to evaluate the conclusions in the paper are present in the paper and/or the Supplementary Materials.

Submitted 3 May 2023
Accepted 12 January 2024
Published 14 February 2024
10.1126/sciadv.adi5501